Co-agonist glycine controls the occurrence of bursts by activating extrasynaptic NMDARs in nigral dopamine neurons

Sofian Ringlet[1,3], Zoraide Motta[2], Laura Vandries[3], Vincent Seutin[3], Kevin Jehasse[4], Laura Caldinelli[2], Loredano Pollegioni[2], and Dominique Engel[1,5]

[1]GIGA-Neurosciences, Laboratory of Molecular Regulation of Neurogenesis, University of Liege, Avenue Hippocrate 15, B-4000 Liege, Belgium
[2]The Protein Factory 2.0 Lab, Dipartimento di Biotecnologie e Scienze della Vita, Università degli Studi dell'Insubria, via Dunant, 3 - 21100 - Varese (VA)
[3]GIGA-Neurosciences, Neurophysiology group, University of Liege, Avenue Hippocrate 15, B-4000 Liege, Belgium
[4]Montefiore Institute of Electrical Engineering and Computer Science, Systems and Modeling research unit at University of Liège, Quartier Polytech 1, allée de la Découverte 10, 4000 Liège 1, Belgium
[5]Lead contact

Correspondence to D.E. (dominique.engel@uliege.be)

Highlights

- NMDAR co-agonist D-serine contributes to the activation of synaptic NMDARs in SNc DA neurons
- Glycine is the preferred co-agonist for activation of extrasynaptic NMDARs and NMDARs implicated in bursting
- NMDAR subunit composition at synaptic and extrasynaptic sites is identical
- Bursts rely mainly on the activation of extrasynaptic NMDARs
- Contribution of co-agonist is unrelated to expression of GluN2 subunit

SUMMARY

Dopamine control of movement initiation is correlated in time to the phasic activity of substantia nigra pars compacta neurons. The participation of NMDARs to the generation of bursts is essential but the mechanisms regulating their level of activation are unknown. Here, we reveal that triheteromeric NMDARs composed of GluN2B and GluN2D subunits are expressed both at synaptic and extrasynaptic sites but are activated by distinct co-agonists. D-serine is predominant for the activation of synaptic NMDARs whereas glycine is for extrasynaptic NMDARs. The pattern of bursts is insensitive to enzymatic depletion of either D-serine or glycine but the latter controls their occurrence. The co-agonist glycine through the activation of extrasynaptic NMDARs plays a central role in the generation of bursts responsible for the enhanced release of dopamine in postsynaptic areas initiating downstream motor-related behavior.

Keywords: excitatory postsynaptic current; NMDA receptor; burst; substantia nigra; patch-clamp; D-serine; glycine; co-agonist

INTRODUCTION

Activity of dopamine (DA) neurons in the substantia nigra pars compacta (SNc) provides essential signal to the dorsal striatum for the control of movement (Jin and Costa, 2010; Howe and Dombeck, 2016; da Silva et al., 2018; Azcorra et al., 2023). The fragility of DA neurons located specifically in this brain region is at the origin of the severe motor deficits expressed in Parkinson's disease (PD) (Hornykiewicz, 2006). The fundamental function ensured by SNc DA neurons is encoded by transitions of their output signal from spontaneous low-frequency action potential (AP) firing to high-frequency bursts of APs. Bursting is a key electrophysiological signal producing an increase of DA release in postsynaptic target areas (Gonon, 1988; Chergui et al., 1994; Ammari et al., 2009), which is temporally correlated to locomotion initiation (Howe and Dombeck, 2016; Khatib and Morris, 2023; Markowitz et al., 2023). Induction of burst firing is operated by N-methyl-D-aspartate receptors (NMDARs) activated by glutamatergic afferents (Chergui et al., 1993; Overton and Clark, 1997; Floresco et al., 2003; Deister et al., 2009; Zweifel et al., 2009) originating from several brain areas but predominantly from the subthalamic nucleus (STN), pedunculopontine nucleus (PPN) and cortex (Watabe-Uchida et al., 2012). A substantial fraction of NMDARs in DA neurons are composed of GluN2B and GluN2D subunits (Brothwell et al., 2008; Morris et al., 2018) as in subthalamic (Swanger et al., 2015) and hippocampal interneurons (Yi et al., 2019; Hansen et al., 2021). GluN2B and GluN2D subunits are commonly expressed at extrasynaptic sites (Momiyama, 2000; Brickley et al., 2003; Lozovaya et al., 2004; Harney et al., 2008) but remarkably these subunits are incorporated into GluN1/GluN2B/GluN2D triheteromers in SN DA neurons found both at synaptic and extrasynaptic sites (Jones and Gibb, 2005). While bursts critically depend on the presence of the GluN1 subunit (Zweifel et al., 2009; Wang et al., 2011), the link

between the integration of the NMDAR-mediated signal and the generation of a burst is fully unknown. This lack of information is surprising since bursts mediate the increased dopamine release which is correlated to movement initiation, a sequence of events that is probably impaired in the context of Parkinson's disease. Bursting activity is observed in vivo in animals (Grace and Bunney, 1984; Otomo et al., 2020) but also in ex vivo tissue by exogenous applications of NMDA in combination to a blocker of SK channels (Seutin et al., 1993; Kitai et al., 1999; Soden et al., 2013; Destreel et al., 2019) or by electrical stimulation of excitatory afferents (Blythe et al., 2007).

In addition to glutamate, a co-agonist such as glycine (Johnson and Ascher, 1987) or D-serine (Kleckner and Dingledine, 1988) is an absolute requirement for NMDAR channel opening (Currás and Pallotta, 1996). While both amino acids have been shown to serve as endogenous agonists at the NMDAR glycine site, the contribution of one or the other is dependent on neuronal development (Le Bail et al., 2015), expression of specific GluN2 subunits (Papouin et al., 2012; Le Bail et al., 2015) and level of synaptic activity (Li et al., 2013). D-serine is generally associated to the synaptic site where GluN2A-containing NMDARs are preferentially expressed, and glycine to the extrasynaptic site where GluN2B-containing NMDARs are present (Papouin et al., 2012). The source of D-serine and glycine seem to be neuronal (Neame et al., 2019; Wong et al., 2020) and astroglial, respectively. The amount of co-agonists in and around the synaptic cleft is tightly controlled by their corresponding synthesis and degrading enzymes and by their specific transporters (Mothet et al., 2015). In SNc DA neurons, both EPCSs and bursts can be potentiated by exogenous co-agonists or by the blockade of glycine uptake (Destreel et al., 2019) indicating that the co-agonist site of NMDARs is not saturated. In addition, blockade of the co-agonist binding-site on NMDARs abolished bursts, revealing the importance of the co-agonist

in this firing pattern (Destreel et al., 2019). However, the identity of the endogenous co-agonist of postsynaptic NMDARs involved in burst generation in DA neurons remains unknown.

In this study, we determined the identity of the co-agonist preponderant for the activation of synaptic and extrasynaptic NMDARs and for the generation of bursting activity in SNc DA neurons. We found that NMDARs from synaptic and extrasynaptic sites are activated by distinct co-agonists, although both of these NMDARs populations are composed of the same set of GluN2 subunits. Interestingly, the pool of NMDARs implicated in bursting and the pool of extrasynaptic NMDARs require the same co-agonist, indicating that the population of NMDARs implicated in bursts is the extrasynaptic NMDARs population. Those findings shed light on the identity of the co-agonist and the NMDAR pool implicated in the generation of bursts in SNc DA neurons.

METHOD DETAILS

Animal Experiments

Experiments on Wistar rats were performed in strict accordance with institutional (protocole 2210, Commission d'Éthique Animale, Université de Liège), national (Comité déontologique), and European guidelines for animal experimentation.

Midbrain slice preparation for patch-clamp recordings

Adolescent 4- to 7-week-old Wistar rats of either sex were anaesthetized with isoflurane (4% in O_2, Matrx VIP 3000, Midmark) and subsequently killed by decapitation. Before anesthesia animals were kept in an oxygen-enriched chamber for fifteen minutes in order to increase cell survival. Brain slices were prepared as

previously described (Bischofberger et al., 2006). Briefly, after decapitation, the brain was rapidly dissected out and immersed in ice-cold slicing solution containing: 87 mM NaCl, 25 mM $NaHCO_3$, 2.5 mM KCl, 1.25 mM NaH_2PO_4, 10 mM D-glucose, 75 mM sucrose, 0.5 mM $CaCl_2$, and 7 mM $MgCl_2$ (pH 7.4 in 95% O_2/5% CO_2, ~325 mOsm). Parasagittal 300 µm (for spontaneous EPSC recordings) or horizontal 250 µm-thick slices (for electrically evoker EPSCS) containing the midbrain were cut using a vibratome (Leica VT-1200, Nussloch, Germany) with a cutting velocity of 0.06 mm/s and a horizontal vibration amplitude of 1.0 mm. Slices containing the SNc were transferred to a storing chamber and allowed to recover at 34°C for 30–45 min. After recovery, slices were kept at room temperature (20 – 25°C) until recording, for up to 4–5 hours.

Patch-clamp recordings

Slices were transferred to a recording chamber and superfused with aCSF containing (in mM): 125 NaCl, 25 $NaHCO_3$, 25 glucose, 2.5 KCl, 1.25 NaH_2PO_4, 2 $CaCl_2$, and 1 $MgCl_2$ (equilibrated with 95% O_2/5% CO_2, Osmolarity ~320 mOsm). DA neurons were visualized using infrared-Dodt gradient contrast (IR-DGC) optics and a 40x objective (numerical aperture 0.75, Zeiss, Oberkochen, Germany) on a Zeiss Axio Examiner.A1 microscope equipped with a CCD camera (C7500-51, Hamamatsu, Japan). The location of the medial terminal (MT) nucleus of the accessory optic tract was used as a reference for the SNc area in horizontal slices. DA neurons were identified in whole-cell using current-clamp and voltage-clamp protocols and post hoc using immunohistochemistry. Selected DA neurons had a voltage rectification with hyperpolarizing current steps, action potentials with long half-width, slow autonomous pacemaking (1-4 Hz) and were positive for tyrosine hydroxylase (**Figure S1**).

Voltage-clamp recordings of DA neurons were conducted with patch pipettes from thick walled borosilicate glass tubing (outer diameter: 2 mm, inner diameter: 1 mm, Hilgenberg, Germany) with a horizontal puller (P-97, Sutter Instruments, Novato, USA). Pipettes were first filled with a potassium gluconate-based internal solution (~1 mm from the tip) and consecutively with a cesium gluconate solution (Wang and Gao, 2010) for whole-cell voltage-clamp recordings. For current-clamp recordings, pipettes were only filled with a potassium-based solution. The potassium gluconate solution consisted of, in mM: 120 K-gluconate, 20 KCl, 2 $MgCl_2$, 4 Na_2ATP, 0.5 NaGTP, 5 Na_2-phosphocreatine, 0.1 EGTA, 10 HEPES and 0.1% biocytin (pH = 7.3; osmolarity: ~302 mOsm) and the cesium solution: 120 Cs-gluconate, 20 CsCl, 2 $MgCl_2$, 4 Na_2ATP, 0.5 NaGTP, 5 Na_2-phosphocreatine, 0.1 EGTA, 10 HEPES, 3 QX-314 and 0.1% biocytin (pH = 7.3; osmolarity: ~306 mOsm). When filled with these solutions, tip resistances were between 3 and 6 MΩ. EPSCs were isolated pharmacologically with $GABA_A$, $GABA_B$ and glycine receptor blockers (picrotoxin, CGP 55485 and strychnine, respectively).

Voltage- and current-clamp recordings were both obtained using a Multiclamp 700B amplifier (Molecular devices, Palo Alto, CA) connected to a PC via a Digidata 1550 interface (Molecular devices). Bridge balance was used to compensate the series resistance (Rs) in current-clamp recordings (Rs <15 MΩ). The current-clamp signal was sampled at 10 kHz. Whole-cell recordings were discarded if the access resistance increased above 15 MΩ for voltage-clamp and above 20 MΩ for current-clamp or if the values varied over 30% during recording. All voltage-clamp and current-clamp recordings were performed at near-physiological temperature (32-34°C).

Bursting activity in SNc DA neurons was generated by bath-applications of NMDA (30 µM) and apamin (300 nM). Hyperpolarizing current injection (from -80 to -140 pA) was

applied to maintain membrane potential in a range (~-60 to -80 mv) that facilitated the occurrence of bursts.

Extracellular synaptic stimulation

Afferent fibers were stimulated electrically using theta-glass pipettes (borosilicate; Hilgenberg) filled with a HEPES-buffered sodium-rich solution. The stimulation pipette was placed rostrally close (within 100 µm) to the recorded DA neuron and short current pulses were applied (200-600 µA, 200-400 ms) for weak (minimal) stimulation. Excitatory afferent fibers originating from the STN were selected using paired-pulse ratio. Paired-pulse facilitation was used to identify fibers from the STN as reported previously (Zheng et al., 2011; Beaudoin et al., 2018). Electrically evoked EPSCs were isolated pharmacologically with $GABA_A$, $GABA_B$ and glycine receptor blockers (picrotoxin, CGP 55485 and strychnine, respectively).

Tonic NMDAR-mediated currents were recorded in the presence of CNQX, picrotoxin, CGP 55485 and strychnine. The amplitude of the tonic current was measured by the baseline shift after 50 µM D-AP5 application.

Synaptic NMDARs were selectively blocked by using the irreversible NMDAR antagonist MK-801 (20 µM) applied for 20 min. Electrically evoked EPSCs (eEPSCs) were recorded at a holding potential of V_{hold} = +40 mV under 0.1 Hz stimulation until stable baseline was obtained. Recording configuration was switched to current-clamp with $V_{membrane}$ ~ -80 mV for 20 min during the bath-application of MK-801 and stimulation was stopped. MK-801 was washed out and recording configuration was switched back to voltage-clamp with V_{hold} = +40 mV. Stimulation was resumed and delivered at 5 Hz for 16 s to block selectively synaptic NMDARs (Liu et al., 2013; Yang

et al., 2017; Koh et al., 2022). Stimulation <10 Hz does not induce measurable extrasynaptic NMDAR-mediated current (Harris and Pettit, 2008).

Drugs and reagents

Picrotoxin (50 µM, Alomone Lab), CGP 55845 (1 µM, Hellobio), strychnine (10 µM, Sigma) and D-AP5 (50 µM, Alomone Lab) were dissolved in doubled distilled water. CNQX was dissolved in DMSO. Picrotoxin was dissolved in 90% ethanol. Biocytin and ProLong Diamond (Life Technologies). Fluorescein Avidin DCS (Labconsult). The remaining chemicals and all salts were purchased from Sigma-Aldrich (Belgium).

Immunohistochemistry

Immunohistochemical analysis for identification of DA neurons was done on 300 µm horizontal or parasagittal slices taken after electrophysiological recordings. Biocytin-filled cells were fixed in 4% paraformaldehyde overnight at 4°C. After washing in phosphate buffer saline (PBS, 0.1 M) and then in PBS containing 10% normal goat serum (NGS) and 0.3% triton X-100, slices were incubated with primary antibody against TH (mouse anti-TH 1:1000, Immunostar 22941, Abcam, UK) in PBS containing 5% goat-serum and 0.3% Triton X-100 for 22 hours at room temperature. Subsequently, slices were rinsed with PBS and incubated with the secondary antibody (goat-anti-mouse-Alexa Fluor 568 1:500, Invitrogen A-11004, Thermo Fischer Scientitfic, Waltham, MA, USA) together with Fluorescein Avidin DCS (1 µl/ml, Vector Laboratories A-2001-5,) in PBS and 0.3% triton X-100 overnight at 4°C. After the final rinsing, slices were mounted on a slide containing a 300 µm iSpacer (SunjinLab #IS307, Hsinchu City, Taiwan) with ProLong Gold Antifade (Invitrogen P36934), and imaged using an FV1000 confocal microscope (Olympus, Tokyo, Japan). Images were

analyzed with Fiji/ImageJ software (https://imagej.net) and Imaris v9.5.1 (Oxford Instruments, Santa Barbara, CA, USA).

To determine the expression of GluN2 subunits in the SNc immunohistochemical analysis was done on 5- to 6-week-old Wistar rats of either sex. Animals were perfused using a peristaltic pump (Watson Marlow, 101U) with PBS (150 mL), followed by PBS containing with 4% PFA (100 mL). Brains were carefully collected, post-fixed in 4% PFA for 24 hours at 4 °C, subsequently stored in sucrose azide 0.01% for 48 hours at 4°C and sliced (40 µm) with a NX70 cryostat (Epredia Belgium, Machelen, Belgium). Slices were exposed to 10% NGS and 0.1% Triton X-100 followed by primary antibody incubations in PBS containing 5% NGS and 0.1% Triton X-100 overnight at 4 °C. Primary antibodies were against GluN2A subunit (rabbit anti-GluN2A 1:200, Alomone AGC-002) combined to mouse anti-TH (1:1000, Immunostar 22941, Abcam, UK), or GluN2B subunit (rabbit anti-GluN2B 1:200, Alomone AGC-003) with mouse anti-TH or GluN2D subunit (rabbit anti-GluN2D 1:200, Alomone AGC-020) with mouse anti-TH in 5% NGS in PBS and 0.1% Triton X-100 overnight at 4 °C. After rinsing, slices were incubated with secondary antibodies (goat anti-mouse alexa Fluor 568 1:500, Invitrogen A-11004 and goat anti-rabbit Alexa Fluor 488 1:400, Invitrogen A-11011) in PBS with 0.1% Triton X-100 for 2 hours at room temperature. Slices were rinsed with PBS and shortly exposed to Dapi (0.5 µg/mL). After mounting with Aqua-poly/mount (Polysciences 18606, Warrington, PA, USA) images were obtained with an FV1000 confocal microscope (Olympus, Tokyo, Japan) using 5x, 40x and 60x oil immersion objectives (N.A. 0.16, 0.8 and 1.4, respectively).

The distribution of the NMDAR subunits within neurons and at their membranes was analyzed using Imaris. Membrane transparency of reconstructed neurons was adjusted by varying the transparency setting implemented in Imaris to differentiate

NMDAR subunits expressed in the cytoplasm (100% transparency - 0% opacity) from NMDAR subunits in the membrane (0% transparency - 100% opacity). TH+ DA neurons were selected around the MT randomly from both hemispheres.

Enzymes

Recombinant wild-type and M213R variants of *Rhodotorula gracilis* D-amino acid oxidase (RgDAAO; EC 1.4.3.3) and recombinant H244K glycine oxidase from *Bacillus subtilis* (BsGO; EC 1.4.3.19) were produced in *E. coli* cells and purified as previously described (Fantinato et al., 2001; Job et al., 2002; Sacchi et al., 2002). The RgDAAO and BsGO preparations had a specific activity of 75 U/mg protein on D-serine as substrate and 2.5 U/mg protein on glycine as substrate, respectively. Hippocampal slices were perfused with RgDAAO (0.2 U/mL) or BsGO (0.2 U/mL) for at least 45 min. For details about RgDAAO and BsGO substrate specificity see (Job et al., 2002; Frattini et al., 2011).

High Performance Liquid Chromatography (HPLC) analysis

Slices containing the substantia nigra were stored in the reserve chamber near-physiological temperature (32-34 °C) using three experimental conditions. The first condition was in physiological saline (aCSF), the second in aCSF + GO (0.2 U mL^{-1}) and the third in aCSF + DAAO (0.2 U mL^{-1}) for 45 minutes. The aCSF collected during all experimental conditions were freeze-dried and then resuspended in 25 mM HCl. Following a neutralization step adding 0.2 M NaOH, the samples were precolumn derivatizated with o-phthaldialdehyde/N-acetyl-L-cysteine in a 1:4 volume ratio of 0.2 M borate, pH 8.2, and 0.2 M sodium phosphate, pH 10. Diastereoisomer derivatives were resolved on a Kinetex EVO C18 reverse-phase column (5 µm, 4.6 x 150 mm; Phenomenex, Bologna, MI, Italy) using a HPLC PU-2089 System (Jasco Europe,

Cremella, LC, Italy) equipped with a fluorescence detector (344/443 nm, gain 1000X), in isocratic conditions (0.1 M sodium acetate buffer, pH 6.2, 3% tetrahydrofuran, 0.7 mL/min flow rate), modified from (Punzo et al., 2016). Identification and quantification of the D- and L-serine and glycine was based on retention times and peak areas, compared with those associated with external standards (calibration curves were built by injecting 0.005-0.2 pmol of standards). To confirm the identity of D-enantiomers, a selective degradation of D-amino acids in aCSF samples was obtained by adding 10 µg of M213R RgDAAO for 4 h at 30 °C. Statistical analyses were performed using GraphPad Prism 9.0.

Data acquisition and analysis

Pulse generation and data acquisition were performed using clampEx (clampEx 10.5, Molecular Devices). Data analysis was performed using pClamp 10.5 (clampFit), Mathematica 13 (Wolfram Research, Champaign, IL), Stimfit (https://github.com/neurodroid/stimfit/wiki/Stimfit) and Prism 8 (GraphPad software, La Jolla, CA). To detect sEPSCs, MiniAnalysis (v6.0.7, Synaptosoft Inc.) was used and every single event was inspected and selected visually. To obtain an averaged EPSC, events were superimposed to the initial phase of the current rise. To measure the parameters of the averaged EPSC (amplitude, 20 – 80% rise time, decay), a short baseline (5 ms) was used immediately preceding the rise of the event. The averaged event was filtered at 2 kHz.

For the analysis of the NMDAR current component of sEPSCs at +40 mV, a dashed vertical line was placed at 10 ms after the onset of the averaged EPSC to evaluate the amplitude of the NMDAR-dependent synaptic current and for eEPSC, it was placed 40 ms after the onset of the event (Li et al., 2013; Jang et al., 2015). At this time point, the AMPAR-current component is back to baseline. The peak amplitude of the AMPAR-

current component was measured at the peak of the averaged EPSC at -70 mV. The horizontal dashed gray lines indicate baseline current. NMDA/AMPA ratio was calculated as the amplitude ratio of EPSC current at +40 mV 10 ms after the onset of the event divided by the amplitude of the EPSC current at -70 mV for EPSC and 40 ms for eEPSC.

Bursts were defined as spontaneously occurring biphasic changes in the membrane potential during which hyperpolarized periods between -60 and -80 mV alternated with depolarized plateau potentials > -60 mV superimposed by APs. This firing activity was reliable and reproducible in the presence of NMDA with the SK channel blocker apamin and hyperpolarizing current injection (Seutin et al., 1993; Hopf et al., 2007; Soden et al., 2013; Destreel et al., 2019).

Statistical analysis

Experimental values are expressed as mean ± standard error of the mean (SEM). Error bars in the figures also indicate SEM. Statistical analysis was performed using Prism 8. Data were tested for normality distribution with Shapiro-wilk and d'Agostino test. Accordingly, paired-data were either tested by ANOVA 1 test followed by a Tukey post hoc test or Friedman test followed by Dunn's post hoc when more than 2 conditions. Unpaired-data were tested with Kruskal-Wallis test followed by Dunn's test. In the case of 2 conditions, either T-test or Wilcoxon test (paired data) and Mann-Withney test (unpaired data) were used. Significance level is given as * < 0.05, ** < 0.01, *** < 0.001 and **** < 0.0001 is displayed in the histograms.

RESULTS

Glycine is the co-agonist activating NMDARs during bursting activity

Bursting in SNc DA neurons is subjected to modulation by distinct co-agonists acting on NMDARs that are not saturated during basal synaptic transmission (Destreel et al., 2019). However, which endogenous co-agonist is predominant to activate NMDARs during phasic activity remains unknown. To identify the co-agonist activating NMDARs implicated in burst generation, enzymatic depletion of the co-agonists was combined to patch-clamp recordings in acute brain slices. DA neurons were identified in current- and voltage-clamp and using post hoc immunohistochemistry for tyrosine hydroxylase (**Figure S1**). Bursting activity was induced by bath application of NMDA and apamin and hyperpolarizing current injection. Slices were incubated for 45 minutes with either D-amino acid oxidase (DAAO) (**Figure 1A**) or glycine oxidase (GO) (**Figure 1B**) to degrade D-serine or glycine, respectively. While the application of DAAO did not affect the profile of the interspike interval (ISI) distribution (**Figure 1C**), burst time course and burst set rate (**Figure 1D–1I; Table 1**), the incubation with GO strongly modified the profile of the ISI distribution (**Figure 1J)** and reduced burst set rate (**Figure 1K–1P; Table 1**). Adding D-serine to DAAO-treated samples modified slightly the ISI distribution profile, increased the depolarizing envelope duration and the number of APs riding on a burst (**Figure 1C–1I; Table 1).** Supplementing glycine to GO-treated samples modified the ISI distribution profile, increased the depolarizing envelope duration and the number of APs riding on a burst but did however not restore the frequency observed in control (**Figure 1K–1P; Table 1**) probably due to the high efficacy of the enzymes. In the absence of the enzymes, the bursting activity remained stable over 45 minutes (**Figure S2; Table 2**). These results indicate that glycine regulate the occurrence of bursts via the activation of NMDARs.

To control for changes in the amount of glycine and D-serine in slices in the presence of either GO or DAAO, concentrations of glycine and D-serine were evaluated using high-performance liquid chromatography (HPLC) experiments. In slices incubated for 45 min with either DAAO (0.2 U mL^{-1}) or GO (0.2 U mL^{-1}), D-serine and glycine concentration was significantly decreased (35.00 ± 12.97% of control; 42.40 ± 11.01% of control respectively), suggesting that the reduction of sEPSCs amplitude is due to a selective reduction of the co-agonist amount (**Figure S3**).

D-serine is the co-agonist activating NMDARs during synaptic transmission

NMDARs are implicated in synaptic transmission in SNc DA neurons (Jang et al., 2015; Pearlstein et al., 2015; Hage et al., 2016) but the nature of the endogenous co-agonist activating the synaptic pool of NMDARs has not been identified. In addition, whether the identity of the co-agonist for synaptic NMDARs and for bursting activity is identical has to be determined. In control conditions, spontaneous excitatory postsynaptic currents (sEPSCs) recorded at +40 mV had a mean amplitude of 10.66 ± 1.63 pA, a rise time of 1.58 ± 0.18 ms and a decay time course of 30.16 ± 2.92 ms (n = 7); at -70 mV, mean amplitude of sEPSCs was 8.84 ± 0.87 pA, rise time 0.56 ± 0.06 ms and decay 6.50 ± 1.47 ms (n = 7). Slices were then treated with either DAAO to degrade D-serine or with GO to reduce the glycine level for 45 min. Treatment with DAAO induced a significant reduction in peak amplitude of the NMDAR-mediated component of sEPSCs at +40 mV (**Figure 2A and 2C**). Addition of exogenous D-serine (100 µM) reversed the effects of DAAO on the amplitude of sEPSCs which was similar to the EPSC amplitude in control. Treatment with GO did not change the amplitude of sEPSCs but supplementation of glycine to GO-treated samples increased the amplitude of sEPSCs which was significantly larger than in control conditions (**Figure**

2B and 2D). Currents at -70 mV, representing largely the activation of AMPARs, were not modified, either in the presence of DAAO or GO. Accordingly, the NMDA/AMPA amplitude ratio was decreased in DAAO and unchanged in the presence of GO (**Figure 2C and 2D**). These results provide evidence that ambient D-serine, but not glycine, maintains synaptic activation of NMDARs in DA neurons under basal synaptic activity. Unexpectedly, the co-agonist activating synaptic NMDARs and NMDARs for bursting differed in their identity. This indicates that the pool of NMDARs implicated in the generation of bursts is different from the pool of synaptic NMDARs.

DA neurons in the SNc receive glutamatergic input principally from the subthalamic nucleus (STN), the pedunculopontine nucleus and motor cortex (Watabe-Uchida et al., 2012). Among these inputs, substantial innervation originates from the STN (Watabe-Uchida et al., 2012). To reveal the identity of the co-agonist in this specific synapse, electrically evoked EPSCs (eEPSCs) were recorded in DA neurons during stimulation of STN excitatory afferent fibers. Synaptic transmission originating from the STN was identified using paired-pulse ratio (see Materials and methods and **Figure S4**) and the stimulation intensity was adjusted to slightly above minimal stimulation to activate the smallest number of fibers. Incubation with DAAO reduced significantly the peak amplitude of the NMDAR-mediated component of eEPSCs at +40 mV and addition of exogenous D-serine (100 µM) reversed the effects of DAAO on the amplitude of eEPSCs (**Figure 3A**). Treatment with GO did not change the mean amplitude of eEPSCs but addition of glycine to GO-treated samples increased the mean amplitude of eEPSCs, which was significantly larger than in control conditions (**Figure 3B**). Currents at -70 mV were neither changed by the treatment with DAAO, nor with GO. Accordingly, the NMDA/AMPA amplitude ratio was statistically decreased in DAAO (**Figure 3C**) and not statistically changed in the presence of GO (**Figure 3D**). These

results obtained on eEPSCs are in line with those observed on sEPSCs and indicate that the same co-agonist is shared among distinct excitatory inputs in DA neurons. In addition, this result further supports that synaptic NMDARs and NMDAR-mediating bursts are activated by distinct co-agonists.

Subunit composition of synaptic NMDARs in nigral DA neurons

A strong association between the nature of the predominant co-agonist in synapses and the expression of a specific GluN2 subunit has been previously established (Fossat et al., 2012; Papouin et al., 2012; Le Bail et al., 2015; Ferreira et al., 2017). D-serine is usually the main co-agonist found to activate synaptic GluN2A-containing NMDARs. In juvenile DA neurons, a high proportion of synaptic NMDARs are GluN1/GluN2B/GluN2D triheteromers and the presence of the GluN2A subunit has not been detected (Brothwell et al., 2008; Morris et al., 2018). Since D-serine is often the co-agonist of GluN2A-containing NMDARs, the subunit composition of NMDARs in DA neurons has been reexamined in adolescent animals in which a potential switch from GluN2B to GluN2A subunits occurring during the second postnatal (Bellone and Nicoll, 2007; Rodenas-Ruano et al., 2012) already happened. Ambient zinc (Zn^{2+}) levels exert a tonic inhibition of EPSCs mediated by GluN2A-containing NMDARs due to a high-affinity binding site for Zn^{2+} specifically on this subunit (Paoletti et al., 1997). To reveal the functional contribution of the GluN2A subunit, we bath-applied the Zn^{2+} chelator tricine (10 mM) to buffer Zn^{2+} (Vergnano et al., 2014; Carta et al., 2018). This treatment did not modify the amplitude of the NMDAR component of eEPSCs at +40 mV (**Figure 4A and 4B**). The subsequent addition of Zn^{2+} (60 µM, corresponding to 300 nM free Zn^{2+}) was also unable to modify the amplitude of eEPSCs. The absence of effect of tricine was also observed for applications of longer duration (**Figure S5**). In contrast,

application of the antagonist of NMDARs containing GluN2B (Ro25-6981, 1 µM) reduced significantly the amplitude of eEPSCs to ~60% of control (**Figure 4C and 4D**). Similarly application of the GluN2D-containing NMDAR antagonist DQP-1105 (20 µM) reduced the amplitude of sEPSCs to ~53% of control (**Figure 4E and 4F**). Weighted decay time constant of EPSCs was not modified by the application of either Ro25-6981 or DQP-1105. The absence of effect on the decay time constant by either Ro25-6981 or DQP-1105 suggests that synaptic NMDARs are essentially composed of a high proportion of GluN1/GluN2B/GluN2D triheteromers making the participation of diheteromeric GluN1/GluN2B and GluN1/GluN2D receptors unlikely (Yi et al., 2019). Taken together, these results indicate that a large fraction of synaptic NMDARs may be GluN1/GluN2B/GluN2D triheteromers in adolescent SN DA neurons as in juvenile tissue (Brothwell et al., 2008) and seem to exclude a switch from Glu2B to GluN2A subunits in DA neurons.

NMDAR GluN2 subunit distribution in nigral DA neurons

The expression of NMDAR subunits in DA neurons was further explored using immunohistochemistry for GluN2A, GluN2B and GluN2D subunits. The distribution of the subunits was determined in TH^+ DA neurons in the region in which DA neurons were selected for patch-clamp recordings (**Figure 5**). Both GluN2B and GluN2D subunits were present in a large majority (~80%) of TH^+ neurons but the GluN2A subunit was only present in ~20% of TH^+ neurons (**Figure 5B and 5C**). Within TH^+ neurons, there were ~3 times more fluorescent dots for GluN2B and GluN2D subunits than for Glun2A subunits (**Figure 5D**). The distribution of the three distinct NMDARs subunits was further examined at higher magnification at the cellular level by taking into account membrane and intracellular locations (**Figure S6**). Immunolabeling for

GluN2B and GluN2D subunits was found predominantly at the membrane (GluN2B membrane, ~75% of the total dots; GluN2D membrane, ~77% of the total dots) in comparison to the intracellular compartment (GluN2B intracellular, ~25% of the total dots; GluN2D intracellular, ~23%). In contrast, the distribution of GluN2A was inverted and found at a high proportion in the intracellular milieu (GluN2A intracellular, ~85%) and at a very low proportion at the membrane (GluN2A membrane, ~15%) (**Figure S6A and S6B**). This expression profile of the GluN2 subunits at the membrane is consistent with the pharmacological data obtained using subunit specific NMDAR blockers (**Figure 4**).

Glycine is the co-agonist activating NMDAR-mediated tonic current

NMDARs are generally concentrated in synapses but are also encountered at extrasynaptic sites (Petralia et al., 2010; Papouin and Oliet, 2014). Activation of extrasynaptic NMDARs by ambient glutamate generates a whole-cell tonic current manifested by the application of the NMDAR blocker D-AP5 (Le Meur et al., 2007). An NMDAR-mediated tonic current has also been described in SN DA neurons (Wild et al., 2015; Morris et al., 2018) but the identity of the co-agonist activating extrasynaptic NMDARs in SNc DA neurons remains undetermined. At +40 mV, the shift in current produced by D-AP5 had an averaged amplitude of ~30 pA which is comparable in amplitude to previous reports for the same neurons (Wild et al., 2015) (**Figure 6A and 6B**). In slices incubated with DAAO, the amplitude of the tonic current was not significantly different from control after application of D-AP5. In contrast, in the presence of GO, the amplitude of the tonic current was reduced to ~46% of control, indicating that reducing the amount of glycine impaired the activation of NMDARs mediating this current. Consistent with previous observations made in other neuronal

types (Papouin et al., 2012), these results support the hypothesis that glycine is the predominant co-agonist acting at extrasynaptic NMDARs. Interestingly, since glycine is the predominant co-agonist for extrasynaptic NMDARs activated during tonic current and is also controlling the occurrence of bursts, extrasynaptic NMDARs might be critical for the generation of bursts.

NMDAR subunit composition of NMDAR-mediated tonic current

Since glycine is the co-agonist for the activation of extrasynaptic NMDARs, the GluN2B subunit is expected to be a component of NMDARs at this location (Papouin et al., 2012). While NMDAR subtypes at synaptic sites generally contain GluN2A subunits, those at extrasynaptic sites contain GluN2B (Dalby and Mody, 2003) and GluN2D subunits (Momiyama, 2000; Brickley et al., 2003). In adolescent SNc DA neurons the subunit composition of extrasynaptic NMDARs is not known. A large proportion could be GluN1/GluN2B/GluN2D triheteromers as suggested for juvenile DA neurons using outside-out patch recordings (Jones and Gibb, 2005). To determine the subunit composition of extrasynaptic NMDARs in DA neurons, subunit specific NMDAR blockers were used. In the presence of Tricine, the magnitude of the tonic current was similar as in control conditions (**Figure 6B**). Adding Zn^{2+} (60 nM) to Tricine did not further modify the current amplitude, indicating that the GluN2A subunit may not compose extrasynaptic NMDARs at the membrane. The GluN2B blocker Ro25-6981 and the GluN2D blocker DQP-1105 reduced significantly the tonic current to ~31% of control and ~26% of control, respectively (**Figure 6C**). These results indicate that extrasynaptic NMDARs may be composed of GluN2B and GluN2D subunits, as observed for juvenile tissue (Jones and Gibb, 2005) and that extrasynaptic, like synaptic sites, may express a high proportion of the same GluN1/GluN2B/GluN2D NMDAR subtype (Brothwell et al., 2008). In addition, these observations confirm that

GluN2B is not enriched in the extrasynaptic membrane and is present both at synaptic and extrasynaptic sites (Harris and Pettit, 2007). Taken together, our results show that despite similar NMDAR subtypes at synaptic and extrasynaptic sites, distinct co-agonists activate NMDARs at synaptic and extrasynaptic sites. The preference of D-serine to act at synaptic NMDARs and glycine at extrasynaptic NMDARs is therefore more probably due to their availability rather than to the expression of a specific GluN2 subunit.

Activation of extrasynaptic NMDARs produce tonic current

It is generally accepted that the tonic NMDAR-mediated current is largely due to the activation of extrasynaptic NMDARs (Le Meur et al., 2007; Fleming et al., 2011). However, tonically activated synaptic NMDARs could also contribute to the tonic current. To evaluate the potential contribution of synaptic NMDARs to the tonic current, we used the irreversible open channel blocker MK-801 to occlude this pool of receptors (Huettner and Bean, 1988; Rosenmund et al., 1993; Liu et al., 2013; Koh et al., 2022). After a 20 min application of MK-801, low frequency stimulation elicited eEPSCs at +40 mV with strongly reduced amplitude to ~30% of control due to the blockade of synaptic NMDARs (**Figure 7A**). The consecutive application of D-AP5 (50 µM) induced a tonic current with an amplitude of ~22 pA that was similar to the amplitude measured without the suppression of synaptic NMDARs (**Figure 7A**). In contrast, the blockade of both synaptic and extrasynaptic NMDARs reduced strongly the amplitude of the tonic current (**Figure 7B**). The absence of a change in the tonic current when synaptic NMDARs are blocked indicates that the pool of extrasynaptic NMDARs sustains the tonic NMDAR-mediated current in DA neurons.

Bursting activity relies on the contribution of extrasynaptic NMDARs

In vivo, bursting activity in SNc DA neurons results from the tonic activation of NMDARs (Chergui et al., 1993). In vitro, spontaneous bursts can be generated by exogenous applications of NMDA and the SK channel blocker apamin but whether synaptic or extrasynaptic NMDARs contribute to this firing activity is not known. To determine the possible participation of synaptic NMDARs to the bursting activity, MK-801 (20 µM) was applied to specifically block this pool of receptors. As shown in the previous recordings, the irreversible open-channel inhibitor reduced strongly the amplitude of eEPSCs at +40 mV to ~26% of control, indicating that a large fraction of synaptic NMDARs were blocked (**Figure 8A**). The recording configuration was then switched from voltage-clamp at +40 mV to current-clamp ($V_{membrane}$ ~ -80 mV) to determine whether the spontaneous bursting activity can be induced. After a short time period (~10 min) to allow stabilization of the membrane potential, NMDA and apamin were bath-applied in combination with small DC current injections. In these conditions, DA neurons exhibited spontaneous bursting activity, similar to the activity recorded without the blockade of synaptic NMDARs (**Figure 1A and 1B and Figure S2A**). These recordings were performed using a K^+-based pipette internal solution and TEA and 4-AP in aCSF to block a majority of potassium conductances in order to stabilize the current baseline at +40 mV in voltage-clamp. TEA and 4-AP were only present in the bath for voltage-clamp recordings and were washed out while switching to current-clamp. The same recordings were repeated using a Cs^+-based internal pipette solution but without potassium conductance blockers. In these conditions, bursting could be generated in a majority of DA neurons (**Figure 8B and 8C**). These results strongly suggest that bursts in DA neurons are elicited mainly by the activation of extrasynaptic NMDARs.

DISCUSSION

The contribution of NMDARs located at synaptic or extrasynaptic sites and the availability of co-agonists within and outside synapses strongly influence the neuronal excitability and the downstream release of neurotransmitter. Here, by using biochemical and electrophysiological experiments, we determined the nature of the co-agonist and the pool of NMDARs implicated in bursts emitted by SNc DA neurons. First, by combining enzymatic depletion of co-agonists and patch-clamp recordings, we identified the co-agonist controlling the occurrence of spontaneous bursts. Second, we uncovered that the co-agonists acting during glutamatergic synaptic transmission and bursting are distinct. Third, we found that the identity of the co-agonist implicated in the activation of extrasynaptic NMDARs and in bursting are identical. Fourth, we showed that the tonic NMDAR-mediated current is predominantly mediated by extrasynaptic NMDARs. Fifth, bursting activity is supported principally by the contribution of extrasynaptic but not synaptic NMDARs. Sixth, immunohistochemical labeling is consistent with electrophysiological recordings and confirms the presence of GluN2B and GluN2D but not GluN2A subunits in the membrane of DA neurons, indicating that the same NMDAR subtype is expressed both at synaptic and extrasynaptic sites. The same NMDAR subunits GluN2B and GluN2D at both locations might therefore invalidate an influence of a co-agonist on the expression of a specific GluN2 subunit or the latter on the distribution of a co-agonist at a given location. Finally, we concluded that bursting in DA neurons is mediated by the activation of extrasynaptic glycine-gated NMDARs.

Location-dependent action of co-agonists

The identity of the co-agonist has been determined for several glutamatergic synapses in distinct principal neurons and brain regions (Panatier et al., 2006; Fossat et al., 2012; Papouin et al., 2012; Curcio et al., 2013; Li et al., 2013; Le Bail et al., 2015; Ferreira et al., 2017). D-serine is engaged in the activation of synaptic NMDAR and the identification of the co-agonist in synapses of DA neurons confirms this rule. In a unique case, glycine has been shown to activate synaptic NMDARs in mature dentate granule cells (Le Bail et al., 2015). The predominant role of D-serine for synaptic NMDARs has been associated to the presence the GluN2A subunit in postsynaptic NMDARs for instance in adolescent cortical layer 5 neurons (Fossat et al., 2012; Meunier et al., 2016) and hippocampal CA1 pyramidal neurons (Papouin et al., 2012; Le Bail et al., 2015; Ferreira et al., 2017). GluN2A is indeed a component of synaptic NMDARs after the maturational switch from GluN2B to GluN2A (Bellone and Nicoll, 2007; Rodenas-Ruano et al., 2012; Sanz-Clemente et al., 2013). In adolescent SNc DA neurons however, synaptic NMDARs are composed of GluN2B and GluN2D subunits as revealed here, an expression pattern already observed at postnatal ages (Brothwell et al., 2008; Suárez et al., 2010; Gibb, 2022). NMDAR-EPSCs were reduced in amplitude to ~60% of control and ~50% of control by the GluN2B-containing NMDAR blocker Ro25-6981 and the GluN2D-containing NMDAR blocker DQP-1105, respectively. These percentages of inhibition are in line with previous studies on midbrain neurons (Harnett et al., 2009; Swanger et al., 2015) and hippocampal interneurons (Yi et al., 2019; Booker et al., 2021) where GluN1/GluN2B/GluN2D triheteromers have been suggested to be present. A small proportion of diheteromeric GluN1/GluN2B or GluN1/GluN2D NMDARs might participate to the synaptic current, but the absence of change of the decay time course of NMDAR-eEPSCs in the presence of either Ro25-6981 or DQP-1105 argues against the presence of these

diheteromeric NMDARs (Brothwell et al., 2008; Perszyk et al., 2016). Diheteromeric GluN1/GluN2B and GluN1/GluN2D NMDARs produce shorter and longer deactivation time constants than triheteromeric receptors, respectively (Yi et al., 2019). Tricine and Zn^{2+} were ineffective to modify NMDAR-EPSC amplitude, indicating the absence of GluN2A in synaptic receptors. Interestingly, some GluN2A subunits were present in a small proportion of SNc DA neurons as revealed by immunohistochemical labelling, but these were mainly located in the intracellular space with only a small proportion at the cell membrane. Together, our results show that the preponderance of D-serine to activate synaptic NMDARs is not accompanied by the postsynaptic presence of GluN2A but either with the expression of GluN2B and GluN2D in SNc DA neurons. In addition, the developmental switch from GluN2B subunits to GluN2A reported for cortical and hippocampal excitatory synapses (Le Bail et al., 2015) does not seem to occur in these neurons.

Enzymatic reduction of glycine revealed that this co-agonist predominates for the activation of extrasynaptic NMDARs in SNc DA neurons which are composed of GluN2B and GluN2D subunits, probably triheteromeres as in the synaptic compartment. A substantial proportion of such NMDAR subtypes is also present in juvenile tissue (Jones and Gibb, 2005; Morris et al., 2018), indicating that these NMDAR subtypes are present throughout development until adolescence. A comparable correspondence between the identity of a co-agonist, glycine, and the expression of the GluN2B subunit has been reported for CA1 pyramidal neurons where glycine activates also preferentially extrasynaptic NMDARs containing GluN2B (Papouin et al., 2012). The presence of GluN2B and GluN2D subunits is generally observed at extrasynaptic sites in distinct types of neurons at postnatal or juvenile ages (Piña-Crespo and Gibb, 2002; Brickley et al., 2003; Lozovaya et al., 2004; Harney et

al., 2008; Sibarov et al., 2018) but also in mature tissue (Momiyama, 2000; Riebe et al., 2016).

Contribution of glycine and extrasynaptic NMDARs to bursting activity in SNc DA neurons

Bursting observed in vivo from SNc DA neurons (Otomo et al., 2020) can be reproduced in slices in the presence of NMDA and apamine (Seutin et al., 1993). The firing in vivo and in vitro is spontaneous and show comparable time courses. Removing endogenous glycine via enzymatic treatment using glycine oxidase (GO) reduced the frequency of bursts, suggesting that this co-agonist, by controlling the activation of a specific pool of NMDARs, modulates burst occurrence. The pivotal role of NMDARs in the generation of bursts has been previously revealed in vivo using pharmacological blockade of NMDARs (Overton and Clark, 1992; Chergui et al., 1993) and in vitro using genetic inactivation of the essential GluN1 subunit specifically in DA neuron (Zweifel et al., 2009; Wang et al., 2011) and showing that inactivated NMDARs induced a similar reduction in burst frequency, as we observed in this work using depletion of glycine. Correlatively, the co-agonist is also preponderant for the activation of extrasynaptic NMDARs underlying for a large part the tonic NMDAR-mediated current (Koh et al., 2022). These results are in line with work showing that in vivo bursting is generated by tonically activated NMDARs (Overton and Clark, 1992; Chergui et al., 1993). Spontaneous bursting activity could be induced after the pharmacological blockade of synaptic NMDARs, further supporting the predominant contribution of extrasynaptic NMDARs to bursting activity. Altogether, these observations strongly suggest that the pool of NMDARs implicated in the generation of bursts and the pool of extrasynaptic NMDARs, both depending on glycine, correspond to the same pool of

NMDARs, joining the observations made in vivo (Overton and Clark, 1992; Chergui et al., 1993). How extrasynaptic NMDARs generate bursts is not known. This pool of receptors could be recruited during temporal summation of excitatory synaptic inputs, mediating slow inactivating NMDAR-EPSCs (Zweifel et al., 2009) due to their slow kinetics (Drotos et al., 2023). Extrasynaptic NMDARs formed by GluN2B and GluN2D could be recruited during glutamate spillover (Lozovaya et al., 2004) when glutamate uptake is saturated (Arnth-Jensen et al., 2002; Wild et al., 2015). The contribution of extrasynaptic NMDARs in the generation of bursts has also been reported for cortical layer 5 pyramidal neurons (Chalifoux and Carter, 2011; Oikonomou et al., 2012) and hippocampal neurons (Herman and Jahr, 2007; Suzuki et al., 2008). Extrasynaptic NMDARs containing GluN2D could induce firing by strengthening the EPSP-spike coupling, as recently shown for GABAergic neurons (Yao et al., 2022).

Segregation of D-serine and glycine within and outside synapses

It is generally admitted that synaptic and extrasynaptic NMDARs have different subunit compositions and functions (Papouin et al., 2012; Papouin and Oliet, 2014). The expression of a specific NMDAR subtype (containing GluN2B and GluN2D but not GluN2A) at both the synaptic and extrasynaptic sites challenges the hypothesized coupling between the identity of the co-agonist and a specific GluN2 NMDAR subunit (Papouin et al., 2012; Le Bail et al., 2015; Ferreira et al., 2017). Despite the similar NMDAR subunit composition within and outside synapses, D-serine is active in the synaptic cleft and glycine at extrasynaptic sites, suggesting that a direct influence of the identity of the co-agonist on the presence of a specific GluN2 subtype is unlikely. Since both sites have the same NMDAR subtype composed of GluN2B and GluN2D and D-serine and glycine have similar affinities for a given GluN2 subunit (Chen et al.,

2008; Traynelis et al., 2010; Ferreira et al., 2017; Hansen et al., 2021), a discrimination between the two co-agonists cannot be operated by NMDARs. Rather, the organization of the microenvironment, the presence of transporters for the co-agonists and the proximity of astrocytic leaflets in the vicinity of NMDARs certainly influences the distribution of the co-agonists. The glycine transporter GLYT1 expressed in the SNc (Cubelos et al., 2005) might maintain a high concentration ratio of D-serine/glycine within the synaptic cleft and a low concentration ratio at the extrasynaptic membrane (Dopico et al., 2006). D-Serine reuptake by ASCT and EAAT transporters is not so efficient since they are not stereoselective and display low to moderate affinity for D-Serine. The mechanisms for the segregation of glycine and D-serine in the extrasynaptic and synaptic compartments, respectively, are not known despite substantial work dedicated to the distinct functions of the tripartite synapse. More work is needed to shed light on the role of the co-agonist compartmentalization.

Exogenous application of glycine potentiates bursts in SNc DA neurons (Destreel et al., 2019) and enzymatic degradation of the co-agonist decreases their frequency as shown here. Glycine is predominant for the activation of extrasynaptic NMDARs which support bursting. These findings represent mechanistic elements that might be considered for pharmacological treatment of Parkinson's disease. Interestingly, stimulating the activation of NMDARs via its co-agonist site could be beneficial during the late phase of PD (Heresco-Levy et al., 2013). In vivo studies and clinical studies showed indeed that administration of sarcosine, a glycine transporter 1 inhibitor, ameliorates some symptoms of PD (Tsai et al., 2014; Frouni et al., 2021, 2022). Increasing the amount of glycine might act at extrasynaptic NMDARs and favor bursting activity by SNc DA neurons in patients with PD, thereby restoring proper movement control.

Acknowledgements: We thank Drs. Laurent Nguyen for critically reading earlier versions of the manuscript, Sandy El Sayed and Laurent Massotte for excellent technical assistance and the collaboration with the GIGA-imaging platform for using the confocal microscope and Imaris. We thank Drs. Jean-Marc Goaillard and Jochen Roeper for reading a final version of the manuscript. This work was supported by grants from the Belgian F.R.S. – F.N.R.S. (FRIA), the Fondation Leon Fredericq, Prix de l'espoir from Marie-José De Ridder and S. R. Fonds facultaires de l'Université de Liège to D.E. Z.M. is a PhD student of the Life Sciences and Biotechnology course at the University of Insubria. L.P. thanks the support from FAR Fondo di Ateneo per la Ricerca.

Competing Interests

The authors report no conflict of interest

Author contributions

Conceptualization, D.E.; Methodology, D.E., L.P., S.R., L.C., ZM and L.V.; Investigation, S.R., L.V., and L.C.; Writing – Original Draft, D.E.; Writing – Review & Editing, D.E. and S.R.; Funding Acquisition, S.R. and D.E.; Resources, V.S. and L.P.; Supervision, D.E.

Data accessibility statement

Raw data are available from the corresponding author on request.

FIGURE LEGENDS

Figure 1. Glycine controls the occurrence of spontaneous bursting

A, Voltage traces of action potential bursts in a SNc DA neuron in the presence of NMDA (30 μM) and apamin (300 nM, left trace), after 45 minutes incubation with DAAO (45 min, 0.2 units/ml; middle trace) and with DAAO supplemented by D-serine (100 μM, right trace). In the dashed squares are enlargements of a single burst.

B, Voltage traces of action potential bursts in a SNc DA neuron in the presence of NMDA (30 μM) and apamin (300 nM, left trace), after 45 minutes incubation with GO (45 min, 0.2 units/ml; middle trace) and with GO supplemented by glycine (1 mM, right trace). In the dashed squares are enlargements of a single burst.

C, Histogram for the distribution of ISI for a DA neuron in control (light grey), with DAAO (light red) and with DAAO supplemented with D-serine (red).

D, Summary plot showing burst duration in control, in the presence of DAAO and in the presence of DAAO supplemented by D-serine (control, 0.90 ± 0.15 s; DAAO, 0.81 ± 0.12 s, $p>0.9999$; DAAO + D-serine, 1.41 ± 0.23 s, $p=0.0373$). Bars are means ± SEM for n=6; Friedman test followed by post hoc Dunn's test.

E, Summary plot of ISI in control, in the presence of DAAO and in the presence of DAAO supplemented by D-serine (control, 96.64 ± 17.92 ms; DAAO, 101.30 ± 27.42 ms, $p=0.9484$; DAAO + D-serine, 93.85 ± 27.52 ms, $p=0.9981$). Bars are means ± SEM for n=6; Anova followed by post hoc Tukey's test.

F, Summary plot showing action potential per burst in control, in the presence of DAAO and in the presence of DAAO supplemented by D-serine (control, 3.61 ± 0.48; DAAO, 4.34 ± 0.72, $p=0.9519$; DAAO + D-serine, 6.16 ± 1.05, $p=0.0014$). Bars are means ± SEM for n=6; Friedman test followed by post hoc Dunn's test.

G, Summary plot showing burst set rate in control, in the presence of DAAO and in the presence of DAAO supplemented by D-serine (control, 0.36 ± 0.08 Hz; DAAO, 0.26 ± 0.04 Hz, p=0.1376; DAAO + D-serine, 0.23 ± 0.03 Hz, p=0.1684). Bars are means ± SEM for n=6; Anova followed by post hoc Tukey's test.

H, Summary plot showing firing rate in control, in the presence of DAAO and in the presence of DAAO supplemented by D-serine (control, 1.10 ± 0.16 Hz; DAAO, 0.98 ± 0.12 Hz, p=0.2435; DAAO + D-serine, 1.21 ± 0.13 Hz, p=0.5762). Bars are means ± SEM for n=6; Anova followed by post hoc Tukey's test.

I, Linear regression graph between firing and burst set rate in control, in the presence of DAAO and in the presence of DAAO supplemented by D-serine (control, R^2=0.81, slope 0.44 ± 0.09; DAAO, R^2=0.62, slope 0.27 ± 0.09; DAAO + D-serine, R^2=0.12, slope 0.07 ± 0.08).

J, ISI histogram demonstrating the distribution of burst activity in control (grey), with GO (light orange) and with GO supplemented with glycine (orange).

K, Summary plot showing burst duration in control, in the presence of GO and in the presence of GO supplemented by glycine (control, 0.92 ± 0.18 s; GO, 1.11 ± 0.23 s, p=0.7976; GO + glycine, 1.90 ± 0.51 s, p=0.0190). Bars are means ± SEM for n=6; Anova followed by post hoc Tukey's test.

L, Summary plot showing ISI in control, in the presence of GO and in the presence of GO supplemented by glycine (control, 107.40 ± 14.93 ms; GO, 100.70 ± 24.69 ms, p=0.9801; GO + glycine, 117.90 ± 31.93 ms, p=0.9521). Bars are means ± SEM for n=6; Anova test followed by post hoc Tukey's test.

M, Summary plot showing action potential per burst in control, in the presence of GO and in the presence of GO supplemented by glycine (control, 2.84 ± 0.22; GO, 2.87 ±

0.29, p>0.9999; GO + glycine, 4.71 ± 1.10, p=0.0281). Bars are means ± SEM for n=6; Friedman test followed by post hoc Tukey's test.

N, Summary plot showing burst set rate in control, in the presence of GO and in the presence of GO supplemented by glycine (control, 0.47 ± 0.06 Hz; GO, 0.17 ± 0.05 Hz, p=0.0042; GO + glycine, 0.19 ± 0.05 Hz, p=0.0053). Bars are means ± SEM for n=8; Anova test followed by post hoc Tukey's test.

O, Summary plot showing firing rate in control, in the presence of GO and in the presence of GO supplemented by glycine (control, 1.21 ± 0.15 Hz; GO, 0.53 ± 0.13 Hz, p=0.0179; GO + glycine, 0.78 ± 0.19 Hz, p=0.2404). Bars are means ± SEM for n=8; Friedman test followed by post hoc Tukey's test.

P, Linear regression graph between firing and burst set rate in control, in the presence of GO and in the presence of GO supplemented by glycine (control, R^2=0.79, slope 0.37 ± 0.08; GO, R^2=0.34, slope 0.53 ± 0.13; GO + glycine, R^2=0.45, slope 0.16 ± 0.07).

Figure 2. D-serine is the main co-agonist of synaptic NMDA receptors in SNc DA neurons during synaptic transmission

***A*,** Averaged traces (~100 events) of spontaneous EPSCs (sEPSCs) at +40 mV (upper traces) and -70 mV (lower traces) in control, DAAO, DAAO+D-serine (100 µM). At the right are superimposed traces from the three conditions.

B, Averaged traces (~100 events) of sEPSCs at +40 mV and -70 mV in control, GO, GO+glycine (300 µM). At the right are superimposed traces from the three conditions. For each condition, traces were recorded in the presence of picrotoxin (50 µM), CGP 55845 (1 µM) and strychnine (10 µM) to block $GABA_A$, $GABA_B$, and Glycine receptors, respectively.

C, Summary bar graph of amplitude at 10 ms after the onset of the event at +40 mV and -70 mV in control, DAAO, and DAAO+D-serine (100µM, left); (+40 mV control, 5.69 ± 1.43 pA; +40 mV DAAO, 2.02 ± 0.36 pA, p=0.0063; +40 mV DAAO + D-serine, 3.28 ± 0.49 pA, p>0.9999); (-70 mV control, -8.84 ± 0.87 pA; -70 mV DAAO, -8.07 ± 0.71 pA, p=0.3815; -70 mV DAAO + D-serine, -8.48 ± 1.03 pA, p=0.7518). Bars are means ± SEM for n=7; Friedman test followed by Dunn's post hoc test for +40 mV recordings and Anova 1 test followed by Tukey's post hoc test for -70 mV recordings. Summary bar graph of the NMDA/AMPA ratio in control, DAAO, and DAAO+D-serine (right); (control, 0.63 ± 0.11; DAAO, 0.26 ± 0.04, p=0.0099; DAAO + D-serine, 0.43 ± 0.08, p>0.9999); (-70 mV control, -8.84 ± 0.87 pA; -70 mV DAAO, -8.07 ± 0.71 pA, p=0.3815; -70 mV DAAO + D-serine, -8.48 ± 1.03 pA, p=0.7518). Bars are means ± SEM for n=7; Friedman test followed by Dunn's post hoc test.

D, Summary bar graph of amplitude at 10 ms after the onset of the event at +40 mV in control, GO and GO + glycine (300µM, left; + 40 mV control, 4.30 ± 0.43 pA; + 40 mV GO, 4.26 ± 0.48 pA, p>0.9999; + 40 mV GO + glycine, 6.01 ± 0.74 pA, p= 0.0485); (-70 mV control, -10.09 ± 1.29 pA; -70 mV GO, -8.80 ± 0.86 pA, p=0.3126; -70 mV GO + glycine, -7.69 ± 0.64 pA, p=0.1260). Bars are means ± SEM for n=7; Friedman test followed by Dunn's post hoc test for +40 mV recordings and Anova 1 test followed by Tukey's post hoc test for -70 mV recordings. Summary bar graph of the NMDA/AMPA ratio in control, GO, and GO + glycine (right, control, 0.45 ± 0.06; GO, 0.45 ± 0.05, p=0.9993; GO + glycine, 0.81 ± 0.06, p= 0.0193). Bars are means ± SEM for n=7; Anova test followed by Tukey's post hoc test.

Figure 3. D-serine is the main co-agonist of synaptic NMDA receptors in SNc DA neurons STN-SNc excitatory synapses

A, Averaged traces (~30 events) of eEPSCs at +40 mV (upper traces) and -70 mV (lower traces) in control, DAAO (45 min; 0.2 units/ml), DAAO+D-serine (100 µM). At the right are superimposed traces from the three conditions. Note the amplitude decrease of the NMDA-eEPSC at +40 mV in DAAO. EPSCs were evoked electrically by stimulation of fibers originating from the STN.

B, Averaged traces (~30 events) of eEPSCs at +40 mV (upper traces) and -70 mV (lower traces) in control, GO (45 min; 0.2 units/ml), GO+glycine (300 µM). At the right are superimposed traces from the three conditions. For each condition traces were recorded in the presence of picrotoxin (50 µM), CGP 55485 (1 µM), CNQX (10 µM), and strychnine (10 µM). Low stimulation levels were used (typically 60 – 320 µA, 80 µs - 600 µs) to evoke eEPSCs.

C, Summary bar graph of amplitude at 40 ms after the onset of the event at +40 mV in control, DAAO, and DAAO+D-serine (100µM, left). (control, 42.07 ± 8.70 pA; DAAO, 25.10 ± 9.65 pA, p=0.0060; DAAO + D-serine, 45.97 ± 15.06 pA, p>0.7516);); (-70 mV control, -85.19 ± 14.46 pA; -70 mV DAAO, -77.85 ± 12.51 pA, p=0.5514; -70 mV DAAO + D-serine, -90.78 ± 20.55 pA, p=0.9659). Bars are means ± SEM for n=7 for control and DAAO, n=5 for DAAO+ D-serine; mixed-effect analysis test followed by Tukey's post hoc test.

Summary bar graph of the NMDA/AMPA ratio in control, DAAO, and DAAO+D-serine (right). (control, 0.48 ± 0.11; DAAO, 0.30 ± 0.09, p=0.0006; DAAO + D-serine, 0.55 ± 0.11, p>0.3696). Bars are means ± SEM for n=7 for control and DAAO, n=5 for DAAO+ D-serine; mixed-effect analysis test followed by Tukey's post hoc test.

D, Summary bar graph of amplitude at 40 ms after the onset of the event at +40 mV in control, GO and GO + glycine (300µM, left; (control, 27.90 ± 6.28 pA; GO, 25.91 ± 7.21 pA, p= 0.9275; GO + glycine, 43.17 ± 8.83 pA, p= 0.0428); (-70 mV control, -67.94 ±

14.34 pA; -70 mV GO, -71.00 ± 18.98 pA, p=0.9480; -70 mV GO + glycine, -65.05 ± 18.00 pA, p=0.9564).. Bars are means ± SEM for n=6; Anova test followed by Tukey's post hoc test. Summary bar graph of the NMDA/AMPA ratio in control, GO, and GO + glycine (right). (control, 0.41 ± 0.08; GO, 0.30 ± 0.07, p=0.4603; GO + glycine, 0.65 ± 0.13, p= 0.0737). Bars are means ± SEM for n=6; Anova test followed by Tukey's post hoc test.

Figure 4. Subunit composition of synaptic NMDARs in nigral DA neurons

A, Averaged eEPSCs (~30 events) recorded from SNc DA neurons at +40 mV in control conditions (black traces), after incubation with Tricine (gray trace) and after Tricine+Zn^{2+} (light grey trace). Low stimulation levels were used (typically 60-320 µA) to evoke eEPSCs. For each condition traces were recorded in the presence of picrotoxin (50 µM), CGP 55485 (1 µM), CNQX (10 µM), and strychnine (10 µM).

B, Bar chart showing the amplitude of the NMDAR-eEPSCs in control conditions (dark grey bar), in Tricine (grey bar) and in Tricine+Zn^{2+} (light grey bar, top); (control, 34.21 ± 2.80 pA; Tricine 33.48 ± 2.99 pA, p= 0.9832; Tricine+Zn^{2+}, 32.40 ± 3.00 pA, p= 0.9005). Bars are means ± SEM for n=8; Anova test followed by Tukey's post hoc test. Bar chart showing the weighted decay time constant of the NMDAR-eEPSCs in control conditions (dark grey bar), in Tricine (grey bar) and in Tricine+Zn^{2+} (light grey bar,bottom); (control, 84.02 ± 14.13 ms; Tricine 84.01 ± 14.28 ms, p>0.999; Tricine+Zn^{2+}, 84.99 ± 12.21 ms, p= 0.9857). Bars are means ± SEM for n=8; Anova test followed by Tukey's post hoc test.

C, Averaged eEPSCs (~30 events) recorded at +40 mV in control conditions (black traces) and in Ro25-6981 (grey traces).

D, Bar chart showing the amplitude of the NMDAR-eEPSCs in control conditions (dark grey bar) and in Ro25-6981 (grey bar,top); (control, 38.60 ± 5.71 pA; Ro25-6981 23.42 ± 4.66 pA, p= 0.0004). Bars are means ± SEM for n=9; Paired T-test. Bar chart showing the weighted decay time constant of the NMDAR-eEPSCs in control conditions (dark grey bar)) and in Ro25-6981 (grey bar,bottom); (control, 91.04 ± 17.93 ms; Ro25-6981, 92.51 ± 16.37 ms, p= 0.8809). Bars are means ± SEM for n=9; Paired T-test.

E, Averaged sEPSCs (~30 events) recorded at +40 mV in control conditions (black traces) and in DQP-1105 (grey traces,top).

F, Bar chart showing the amplitude of the NMDAR-eEPSCs in control conditions (dark grey bar) and in DQP-1105 (grey bar,top); (control, 35.99 ± 3.19 pA; DQP-1105, 19.38 ± 4.95 pA, p= 0.0065). Bars are means ± SEM for n=7; Paired T-test. Bar chart showing the decay of the NMDAR-eEPSCs in control conditions (dark grey bar) and in Ro25-6981 (grey bar,bottom); (control, 68.84 ± 24.38 ms; Ro25-6981, 76.05 ± 26.30 ms, p= 0.5811). Bars are means ± SEM for n=7; Paired T-test.

Figure 5. Expression of GluN2 NMDAR subunits in nigral DA neurons

A, Light-micrograph of substantia nigra, showing immunolabeling for tyrosine hydroxylase (TH). MT refers to medial terminal nucleus of the accessory optic tract and has been used as an orientation point for the localization of the SNc.

B, Confocal light-micrograph of TH immunoreactivity (left), GluN2A immunoreactivity (top, center), GluN2B immunoreactivity (middle, center), GluN2D immunoreactivity (bottom, center), and overlay of GluN2A and TH (top, right), GluN2B and TH (middle, right) and GluN2D and TH (bottom, right); single confocal sections.

C, Summary bar graph of percentage of TH^+ neurons expressing GluN2A, GluN2B or GluN2D (GluN2A, 21.54 ± 3.55 %; GluN2B, 82.76 ± 2.90 pA, p<0.0001; GluN2D, 71.71

± 4.66 %, p= 0.0003). Bars are means ± SEM for n=7 (N=14); Kruskal-Wallis test followed by a post hoc Dunn's test.

D, Summary bar graph of the average number of fluorescent dots of either GluN2A, GluN2B or GluN2D in a TH^+ neuron (GluN2A, 1.23 ± 0.0.35; GluN2B, 5.07 ± 0.85, p= 0.0043; GluN2D, 6.26 ± 0.1.22, p=0.0009). Bars are means ± SEM for n=7 (N=14); Kruskal-Wallis test followed by a post hoc Dunn's test.

Figure 6. Glycine gates extrasynaptic NMDARs in nigral DA neurons

A, Tonic NMDAR-mediated current in control conditions (top), during incubation of DAAO (middle) and in GO (bottom) revealed by the current shift induced by the application of D-AP5 (50 µM) at a holding potential of +40 mV. Dashed red line indicate amplitude of holding current without D-AP5.

B, Tonic NMDAR-mediated current in tricine (10 mM, top), in tricine + Zn^{2+} (10 mM + 30 mM, second from top), in Ro25-6981 (1 µM, third from top) and in DQP-1105 (20 µM, bottom) revealed by the current shift induced by the application of D-AP5 (50 µM) at a holding potential of +40 mV. Dashed red line indicate amplitude of holding current without D-AP5.

C, Summary bar graph of the mean peak amplitude of the NMDAR-mediated tonic current in control, DAAO, GO, Tricine, Tricine + Zn^{2+},Ro25-6981 and DQP-1105; (control, -26.47 ± 2.51 pA; DAAO, -21.26 ± 3.52 pA, p>0.9999; GO, -12.06 ± 3.03 pA, p=0.0295; Tricine, -22.60 ± 4.22 pA, p>0.9999; Tricine + Zn^{2+}, -23.10 ± 3.24 pA, p>0.9999; Ro25-6981, -8.09 ± 2.35 pA, p=0.0015; DQP-1105, -6.90 ± 3.45 pA, p=0.0017). Bars are means ± SEM for control (n=11), DAAO (n=10), GO (n=12), Tricine (n=11), Tricine + Zn^{2+} (n=13), Ro25-6981 (n=11) and DQP-1105 (n=11); Kruskal-Wallis test followed by a post hoc Dunn's test.

Figure 7. Tonic NMDAR-mediated current is mediated by extrasynaptic NMDARs

A, Experimental design to block synaptic NMDARs using MK-801 (left). Control electrically evoked EPSCs (eEPSCs) at V_{hold} = +40 mV under low stimulation frequency (0.1 Hz) in voltage-clamp. Switch to current-clamp ($V_{membrane}$ ~ -80 mV) for ~20 min during the application of MK-801 (40 µM). Washout of MK-801 and switch back to V_{hold} = +40 mV. Stimulation was resumed using a frequency of 5 Hz for 16 s (Liu et al., 2013; Yang et al., 2017; Koh et al., 2022). Note the blockade of synaptic NMDARs. Neuron was kept at V_{hold} = +40 mV and D-AP5 was applied. During inhibition of synaptic NMDARs, CNQX (50 µM), pticrotoxin (50 µM), CGP (1 µM) and strychnine (10 µM) were applied. For tonic current recording, CNQX, picrotoxin, CGP and strychnine were present in the bath.

B, Experimental design to block both synaptic NMDARs and extrasynaptic NMDARs using MK-801 (left). During application of MK-801, holding potential was kept at +40 mV. Stimulation frequency was 0.2 Hz. Note the almost absence of the tonic current after application of D-AP5.

C, Summary bar graph of peak amplitude of the tonic NMDAR-mediated current neuron (control, -26.47 ± 2.51 pA; +MK-801 (syn), -21.84 ± 2.30 pA, p= 0.3391; +MK-801 (syn + extrasyn), -10.64 ± 1.97 pA, p=0.0004). Bars are means ± SEM for control (n=11), +MK-801 (syn) (n=9), +MK-801 (syn + extrasyn) (n=7) ; Anova test followed by a post hoc Tukey's test.

Figure 8. Bursting activity mediated by extrasynaptic NMDARs

A, Blockade of synaptic NMDARs using MK-801. Control eEPSCs at Vhold = +40 mV under low stimulation frequency (0.1 Hz) in voltage-clamp. Switch to current-clamp

($V_{membrane}$ ~ -70 mV) for ~20 min during the application of MK-801 (40 µM). Washout of MK-801 and switch back to Vhold = +40 mV. Stimulation was at 5 Hz for 16 s. Bursting activity (right) recorded in current-clamp induced by application of NMDA and apamin.

B, ISI histogram demonstrating the distribution of burst activity in control (light grey), with blockade of synaptic NMDARs (dark grey).

C, Summary plot showing burst duration in control and after the blockade of synaptic NMDARs (control, 1.10 ± 0.18 s; $_{syn}$NMDARs blocked, 1.43 ± 0.29 ms, p=0.2824). Bars are means ± SEM for n=8 control and n=6 $_{syn}$NMDARs blocked; Mann-Whitney test.

D, Summary plot showing ISI in control and after the blockade of synaptic NMDARs (control, 111.70 ± 14.68 ms; $_{syn}$NMDARs blocked, 131.70 ± 14.98 ms, p=0.3670). Bars are means ± SEM for n=8 control and n=6 $_{syn}$NMDARs blocked; unpaired T-test.

E, Summary plot showing action potential per burst in in control and after the blockade of synaptic NMDARs (control, 2.77 ± 0.25; $_{syn}$NMDARs blocked, 2.20 ± 0.30, p=0.1636). Bars are means ± SEM for n=8 control and n=6 $_{syn}$NMDARs blocked; unpaired T-test.

F, Summary plot showing burst set rate in control and after the blockade of synaptic NMDARs (control, 0.36 ± 0.05 Hz; $_{syn}$NMDARs blocked, 0.35 ± 0.08 Hz, p=0.9106). Bars are means ± SEM for n=8 control and n=6 $_{syn}$NMDARs blocked; unpaired T-test.

G, Summary plot showing firing rate in control and after the blockade of synaptic NMDARs (control, 0.9125 ± 0.13 Hz; $_{syn}$NMDARs blocked, 0.69 ± 0.10 Hz, p=0.2824). Bars are means ± SEM for n=8 control and n=6 $_{syn}$NMDARs blocked; Mann-Whitney test.

H, Linear regression graph between firing and burst set rate in control and after the blockade of synaptic NMDAR (control, R^2=0.80, slope 0.37 ± 0.08; $_{syn}$NMDARs blocked, R^2=0.95, slope 0.40 ± 0.05).

I, Pie charts representing the percentage of neurons bursting after the blockade of synaptic NMDARs with an intracellular K-gluconate solution or Cesium-gluconate solution.

REFERENCES

Ammari R, Lopez C, Fiorentino H, Gonon F, Hammond C (2009) A mouse juvenile or adult slice with preserved functional nigro-striatal dopaminergic neurons. Neuroscience 159:3–6.

Arnth-Jensen N, Jabaudon D, Scanziani M (2002) Cooperation between independent hippocampal synapses is controlled by glutamate uptake. Nat Neurosci 5:325–331.

Azcorra M, Gaertner Z, Davidson C, He Q, Kim H, Nagappan S, Hayes CK, Ramakrishnan C, Fenno L, Kim YS, Deisseroth K, Longnecker R, Awatramani R, Dombeck DA (2023) Unique functional responses differentially map onto genetic subtypes of dopamine neurons. Nat Neurosci 26:1762–1774.

Beaudoin G, Gomez J, Perkins J, Bland J, Petko A, Paladini C (2018) Cocaine selectively reorganizes excitatory inputs to substantia Nigra pars compacta dopamine neurons. Journal of Neuroscience 38:1151–1159.

Bellone C, Nicoll RA (2007) Rapid Bidirectional Switching of Synaptic NMDA Receptors. Neuron 55:779–785.

Bischofberger J, Engel D, Li L, Geiger JRP, Jonas P (2006) Patch-clamp recording from mossy fiber terminals in hippocampal slices. Nat Protoc 1:1–7.

Blythe SN, Atherton JF, Bevan MD (2007) Synaptic Activation of Dendritic AMPA and NMDA Receptors Generates Transient High-Frequency Firing in Substantia Nigra Dopamine Neurons In Vitro. J Neurophysiol 97:2837–2850.

Booker SA, Sumera A, Kind PC, Wyllie DJA (2021) Contribution of NMDA Receptors to Synaptic Function in Rat Hippocampal Interneurons. eNeuro 8:1–16.

Brickley SG, Misra C, Mok MHS, Mishina M, Cull-Candy SG (2003) NR2B and NR2D subunits coassemble in cerebellar Golgi cells to form a distinct NMDA receptor subtype restricted to extrasynaptic sites. J Neurosci 23:4958–4966.

Brothwell SLC, Barber JL, Monaghan DT, Jane DE, Gibb AJ, Jones S (2008) NR2B- and NR2D-containing synaptic NMDA receptors in developing rat substantia nigra pars compacta dopaminergic neurones. J Physiol 586:739–750.

Carta M, Srikumar BN, Gorlewicz A, Rebola N, Mulle C (2018) Activity-dependent control of NMDA receptor subunit composition at hippocampal mossy fibre synapses. Journal of Physiology 596:703–716.

Chalifoux JR, Carter AG (2011) Glutamate spillover promotes the generation of NMDA spikes. Journal of Neuroscience 31:16435–16446.

Chen PE, Geballe MT, Katz E, Erreger K, Livesey MR, O'toole KK, Le P, Lee CJ, Snyder JP, Traynelis SF, Wyllie DJA (2008) Modulation of glycine potency in rat recombinant NMDA receptors containing chimeric NR2A/2D subunits expressed in Xenopus laevis oocytes. Journal of Physiology 586:227–245.

Chergui K, Charléty PJ, Akaoka H, Saunier CF, Brunet J -L, Buda M, Svensson TH, Chouvet G (1993) Tonic Activation of NMDA Receptors Causes Spontaneous Burst Discharge of Rat Midbrain Dopamine Neurons In Vivo. Eur J Neurosci 5:137–144.

Chergui K, Suaud-Chagny MF, Gonon F (1994) Nonlinear relationship between impulse flow, dopamine release and dopamine elimination in the rat brain in vivo. Neuroscience 62:641–645.

Cubelos B, Giménez C, Zafra F (2005) Localization of the GLYT1 glycine transporter at glutamatergic synapses in the rat brain. Cereb Cortex 15:448–459.

Curcio L, Podda M V., Leone L, Piacentini R, Mastrodonato A, Cappelletti P, Sacchi S, Pollegioni L, Grassi C, D'Ascenzo M (2013) Reduced d-serine levels in the

nucleus accumbens of cocaine-treated rats hinder the induction of NMDA receptor-dependent synaptic plasticity. Brain 136:1216–1230.
Currás MC, Pallotta BS (1996) Single-channel evidence for glycine and NMDA requirement in NMDA receptor activation. Brain Res 740:27–40.
da Silva JA, Tecuapetla F, Paixão V, Costa RM (2018) Dopamine neuron activity before action initiation gates and invigorates future movements. Nature 554:244–248.
Dalby NO, Mody I (2003) Activation of NMDA receptors in rat dentate gyrus granule cells by spontaneous and evoked transmitter release. J Neurophysiol 90:786–797.
Deister CA, Teagarden MA, Wilson CJ, Paladini CA (2009) An intrinsic neuronal oscillator underlies dopaminergic neuron bursting. J Neurosci 29:15888–15897.
Destreel G, Seutin V, Engel D (2019) Subsaturation of the N-methyl-D-aspartate receptor glycine site allows the regulation of bursting activity in juvenile rat nigral dopamine neurons. Eur J Neurosci 50:3454–3471.
Dopico JG, González-Hernández T, Pérez IM, García IG, Abril AM, Inchausti JO, Rodríguez Díaz M (2006) Glycine release in the substantia nigra: Interaction with glutamate and GABA. Neuropharmacology 50:548–557.
Drotos A, Herrera Y, Zarb R, Roberts M (2023) GluN2D-containing NMDA receptors enhance temporal integration in VIP neurons in the inferior colliculus. bioRxiv preprint:1–13.
Fantinato S, Pollegioni L, Pilone S. M (2001) Engineering, expression and purification of a His-tagged chimeric D-amino acid oxidase from Rhodotorula gracilis. Enzyme Microb Technol 29:407–412.
Ferreira JS, Papouin T, Ladépêche L, Yao A, Langlais VC, Bouchet D, Dulong J, Mothet JP, Sacchi S, Pollegioni L, Paoletti P, Oliet SH, Groc L (2017) Co-agonists differentially tune GluN2B-NMDA receptor trafficking at hippocampal synapses. Elife 6:1–22.
Fleming TM, Scott V, Naskar K, Joe N, Brown CH, Stern JE (2011) State-dependent changes in astrocyte regulation of extrasynaptic NMDA receptor signalling in neurosecretory neurons. J Physiol 589:3929–3941.
Floresco SB, West AR, Ash B, Moorel H, Grace AA (2003) Afferent modulation of dopamine neuron firing differentially regulates tonic and phasic dopamine transmission. Nat Neurosci 6:968–973.
Fossat P, Turpin FR, Sacchi S, Dulong J, Shi T, Rivet JM, Sweedler J V., Pollegioni L, Millan MJ, Oliet SHR, Mothet JP (2012) Glial D-serine gates NMDA receptors at excitatory synapses in prefrontal cortex. Cerebral Cortex 22:595–606.
Frattini L, Rosini E, Pollegioni L, Pilone MS (2011) Analyzing the d-amino acid content in biological samples by engineered enzymes. Journal of Chromatography B 879:3235–3239.
Frouni I, Belliveau S, Maddaford S, Nuara SG, Gourdon JC, Huot P (2021) Effect of the glycine transporter 1 inhibitor ALX-5407 on dyskinesia, psychosis-like behaviours and parkinsonism in the MPTP-lesioned marmoset. Eur J Pharmacol 910:174452.
Frouni I, Kang W, Bédard D, Belliveau S, Kwan C, Hadj-Youssef S, Bourgeois-Cayer É, Ohlund L, Sleno L, Hamadjida A, Huot P (2022) Effect of glycine transporter 1 inhibition with bitopertin on parkinsonism and L-DOPA induced dyskinesia in the 6-OHDA-lesioned rat. Eur J Pharmacol 929:175090.
Gibb AJ (2022) Allosteric antagonist action at triheteromeric NMDA receptors. Neuropharmacology 202:1–7.

Gonon FG (1988) Nonlinear relationship between impulse flow and dopamine released by rat midbrain dopaminergic neurons as studied by in vivo electrochemistry. Neuroscience 24:19–28.
Grace AA, Bunney BS (1984) The control of firing pattern in nigral dopamine neurons: burst firing. J Neurosci 4:2877–2890.
Hage TA, Sun Y, Khaliq ZM (2016) Electrical and Ca2+ signaling in dendritic spines of substantia nigra dopaminergic neurons. Elife 5:1–26.
Hansen KB, Wollmuth LP, Bowie D, Furukawa H, Menniti FS, Sobolevsky AI, Swanson GT, Swanger SA, Greger IH, Nakagawa T, McBain CJ, Jayaraman V, Low CM, Dell'Acqua ML, Diamond JS, Camp CR, Perszyk RE, Yuan H, Traynelis SF (2021) Structure, Function, and Pharmacology of Glutamate Receptor Ion Channels. Pharmacol Rev 73:1469–1658.
Harnett MT, Bernier BE, Ahn K-C, Morikawa H (2009) Burst-timing-dependent plasticity of NMDA receptor-mediated transmission in midbrain dopamine neurons. Neuron 62:826–838.
Harney SC, Jane DE, Anwyl R (2008) Extrasynaptic NR2D-containing NMDARs are recruited to the synapse during LTP of NMDAR-EPSCs. Journal of Neuroscience 28:11685–11694.
Harris AZ, Pettit DL (2007) Extrasynaptic and synaptic NMDA receptors form stable and uniform pools in rat hippocampal slices. Journal of Physiology 584:509–519.
Harris AZ, Pettit DL (2008) Recruiting Extrasynaptic NMDA Receptors Augments Synaptic Signaling. J Neurophysiol 99:524–533.
Heresco-Levy U, Shoham S, Javitt DC (2013) Glycine site agonists of the N-methyl-d-aspartate receptor and Parkinson's disease: A hypothesis. Movement Disorders 28:419–424.
Herman M, Jahr C (2007) Extracellular glutamate concentration in hippocampal slice. J Neurosci 27:9736–9741.
Hopf FW, Martin M, Chen BT, Bowers MS, Mohamedi MM, Bonci A (2007) Withdrawal From Intermittent Ethanol Exposure Increases Probability of Burst Firing in VTA Neurons In Vitro. J Neurophysiol 98:2297–2310.
Hornykiewicz O (2006) The discovery of dopamine deficiency in the parkinsonian brain. In: Parkinson's Disease and Related Disorders, pp 9–15. Vienna: Springer Vienna.
Howe MW, Dombeck DA (2016) Rapid signalling in distinct dopaminergic axons during locomotion and reward. Nature 535:505–510.
Huettner JE, Bean BP (1988) Block of N-methyl-D-aspartate-activated current by the anticonvulsant MK-801: selective binding to open channels. Proceedings of the National Academy of Sciences 85:1307–1311.
Jang M, Um KB, Jang J, Kim HJ, Cho H, Chung S, Park MK (2015) Coexistence of glutamatergic spine synapses and shaft synapses in substantia nigra dopamine neurons. Sci Rep 5:14773.
Jin X, Costa RM (2010) Start/stop signals emerge in nigrostriatal circuits during sequence learning. Nature 466:457–462.
Job V, Molla G, Pilone MS, Pollegioni L (2002) Overexpression of a recombinant wild-type and His-tagged *Bacillus subtilis* glycine oxidase in *Escherichia coli*. Eur J Biochem 269:1456–1463.
Johnson JW, Ascher P (1987) Glycine potentiates the NMDA response in cultured mouse brain neurons. Nature 325:529–531.
Jones S, Gibb AJ (2005) Functional NR2B- and NR2D-containing NMDA receptor channels in rat substantia nigra dopaminergic neurones. J Physiol 569:209–221.

Khatib D, Morris G (2023) Spontaneous behaviour is shaped by dopamine in two ways. Nature 614:36–37.
Kitai ST, Shepard PD, Callaway JC, Scroggs R (1999) Afferent modulation of dopamine neuron firing patterns. Curr Opin Neurobiol 9:690–697.
Kleckner NW, Dingledine R (1988) Requirement for Glycine in Activation of NMDA-Receptors Expressed in Xenopus Oocytes. Science 241:835–837.
Koh W et al. (2022) Astrocytes Render Memory Flexible by Releasing D-Serine and Regulating NMDA Receptor Tone in the Hippocampus. Biol Psychiatry 91:740–752.
Le Bail M, Martineau M, Sacchi S, Yatsenko N, Radzishevsky I, Conrod S, Ait Ouares K, Wolosker H, Pollegioni L, Billard J-M, Mothet J-P (2015) Identity of the NMDA receptor coagonist is synapse specific and developmentally regulated in the hippocampus. Proc Natl Acad Sci U S A 112:E204-13.
Le Meur K, Galante M, Angulo MC, Audinat E (2007) Tonic activation of NMDA receptors by ambient glutamate of non-synaptic origin in the rat hippocampus. J Physiol 580:373–383.
Li Y, Sacchi S, Pollegioni L, Basu AC, Coyle JT, Bolshakov VY (2013) Identity of endogenous NMDAR glycine site agonist in amygdala is determined by synaptic activity level. Nat Commun 4:1760.
Liu D dan, Yang Q, Li S tian (2013) Activation of extrasynaptic NMDA receptors induces LTD in rat hippocampal CA1 neurons. Brain Res Bull 93:10–16.
Lozovaya NA, Grebenyuk SE, Tsintsadze TSh, Feng B, Monaghan DT, Krishtal OA (2004) Extrasynaptic NR2B and NR2D subunits of NMDA receptors shape ‘superslow’ afterburst EPSC in rat hippocampus. J Physiol 558:451–463.
Markowitz JE, Gillis WF, Jay M, Wood J, Harris RW, Cieszkowski R, Scott R, Brann D, Koveal D, Kula T, Weinreb C, Osman MAM, Pinto SR, Uchida N, Linderman SW, Sabatini BL, Datta SR (2023) Spontaneous behaviour is structured by reinforcement without explicit reward. Nature 614:108–117.
Meunier CNJ, Dallérac G, Le Roux N, Sacchi S, Levasseur G, Amar M, Pollegioni L, Mothet J-P, Fossier P (2016) D-Serine and Glycine Differentially Control Neurotransmission during Visual Cortex Critical Period. PLoS One 11:1–20.
Momiyama A (2000) Distinct synaptic and extrasynaptic NMDA receptors identified in dorsal horn neurones of the adult rat spinal cord. Journal of Physiology 523:621–628.
Morris PG, Mishina M, Jones S (2018) Altered Synaptic and Extrasynaptic NMDA Receptor Properties in Substantia Nigra Dopaminergic Neurons From Mice Lacking the GluN2D Subunit. Front Cell Neurosci 12:1–12.
Mothet J-P, Le Bail M, Billard J-M (2015) Time and space profiling of NMDA receptor co-agonist functions. J Neurochem 135:210–225.
Neame S, Safory H, Radzishevsky I, Touitou A, Marchesani F, Marchetti M, Kellner S, Berlin S, Foltyn VN, Engelender S, Billard JM, Wolosker H (2019) The NMDA receptor activation by D-serine and glycine is controlled by an astrocytic Phgdh-dependent serine shuttle. Proc Natl Acad Sci U S A 116:20736–20742.
Oikonomou KD, Short SM, Rich MT, Antic SD (2012) Extrasynaptic glutamate receptor activation as cellular bases for dynamic range compression in pyramidal neurons. Front Physiol:1–22.
Otomo K, Perkins J, Kulkarni A, Stojanovic S, Roeper J, Paladini CA (2020) In vivo patch-clamp recordings reveal distinct subthreshold signatures and threshold dynamics of midbrain dopamine neurons. Nat Commun 11:1–15.

Overton P, Clark D (1992) Iontophoretically Administered Drugs Acting at the N-Methyl-D-Aspartate Receptor Modulate Burst Firing in A9 Dopamine Neurons in the Rat. Synapse 10:131–140.
Overton P, Clark D (1997) Burst firing in midbrain dopaminergic neurons. Brain Res Rev 25:312–334.
Panatier A, Theodosis DT, Mothet JP, Touquet B, Pollegioni L, Poulain DA, Oliet SHR (2006) Glia-Derived d-Serine Controls NMDA Receptor Activity and Synaptic Memory. Cell 125:775–784.
Paoletti P, Ascher P, Neyton J (1997) High-Affinity Zinc Inhibition of NMDA NR1–NR2A Receptors. Journal of Neuroscience 17:5711–5725.
Papouin T, Ladépêche L, Ruel J, Sacchi S, Labasque M, Hanini M, Groc L, Pollegioni L, Mothet JP, Oliet SHR (2012) Synaptic and extrasynaptic NMDA receptors are gated by different endogenous coagonists. Cell 150:633–646.
Papouin T, Oliet SHR (2014) Organization, Control and function of extrasynaptic NMDA receptors. Philosophical Transactions of the Royal Society B: Biological Sciences 369:18–21.
Pearlstein E, Gouty-Colomer L-A, Michel FJ, Cloarec R, Hammond C (2015) Glutamatergic synaptic currents of nigral dopaminergic neurons follow a postnatal developmental sequence. Front Cell Neurosci 9:210.
Perszyk RE, DiRaddo JO, Strong KL, Low CM, Ogden KK, Khatri A, Vargish GA, Pelkey KA, Tricoire L, Liotta DC, Smith Y, McBain CJ, Traynelis SF (2016) GluN2D-containing N-methyl-D-aspartate receptors mediate synaptic transmission in hippocampal interneurons and regulate interneuron activity. Mol Pharmacol 90:689–702.
Petralia RS, Wang YX, Hua F, Yi Z, Zhou A, Ge L, Stephenson FA, Wenthold RJ (2010) Organization of NMDA receptors at extrasynaptic locations. Neuroscience 167:68–87.
Piña-Crespo JC, Gibb AJ (2002) Subtypes of NMDA receptors in new-born rat hippocampal granule cells. J Physiol 541:41–64.
Punzo D et al. (2016) Age-Related Changes in d-Aspartate Oxidase Promoter Methylation Control Extracellular d-Aspartate Levels and Prevent Precocious Cell Death during Brain Aging. The Journal of Neuroscience 36:3064–3078.
Riebe I, Seth H, Culley G, Dósa Z, Radi S, Strand K, Fröjd V, Hanse E (2016) Tonically active NMDA receptors - a signalling mechanism critical for interneuronal excitability in the CA1 stratum radiatum. Eur J Neurosci 43:169–178.
Rodenas-Ruano A, Chávez AE, Cossio MJ, Castillo PE, Zukin RS (2012) REST-dependent epigenetic remodeling promotes the developmental switch in synaptic NMDA receptors. Nat Neurosci 15:1382–1390.
Rosenmund C, Clements JD, Westbrook GL (1993) Nonuniform Probability of Glutamate Release at a Hippocampal Synapse. Science (1979) 262:754–757.
Sacchi S, Lorenzi S, Molla G, Pilone MS, Rossetti C, Pollegioni L (2002) Engineering the Substrate Specificity ofd-Amino-acid Oxidase. Journal of Biological Chemistry 277:27510–27516.
Sanz-Clemente A, Nicoll RA, Roche KW (2013) Diversity in NMDA receptor composition: Many regulators, many consequences. Neuroscientist 19:62–75.
Seutin V, Johnson SW, North RA (1993) Apamin increases NMDA-induced burst-firing of rat mesencephalic dopamine neurons. Brain Res 630:341–344.
Sibarov DA, Stepanenko YD, Silantiev I V., Abushik PA, Karelina T V., Antonov SM (2018) Developmental Changes of Synaptic and Extrasynaptic NMDA Receptor

Expression in Rat Cerebellar Neurons In Vitro. Journal of Molecular Neuroscience 64:300–311.
Soden ME, Jones GL, Sanford CA, Chung AS, Güler AD, Chavkin C, Luján R, Zweifel LS (2013) Disruption of Dopamine Neuron Activity Pattern Regulation through Selective Expression of a Human KCNN3 Mutation. Neuron 80:997–1009.
Suárez F, Zhao Q, Monaghan DT, Jane DE, Jones S, Gibb AJ (2010) Functional heterogeneity of NMDA receptors in rat substantia nigra pars compacta and reticulata neurones. Eur J Neurosci 32:359–367.
Suzuki T, Kodama S, Hoshino C, Izumi T, Miyakawa H (2008) A plateau potential mediated by the activation of extrasynaptic NMDA receptors in rat hippocampal CA1 pyramidal neurons. Eur J Neurosci 28:521–534.
Swanger SA, Vance KM, Pare JF, Sotty F, Fog K, Smith Y, Traynelis SF (2015) NMDA receptors containing the GluN2D subunit control neuronal function in the subthalamic nucleus. Journal of Neuroscience 35:15971–15983.
Traynelis SF, Wollmuth LP, McBain CJ, Menniti FS, Vance KM, Ogden KK, Hansen KB, Yuan H, Myers SJ, Dingledine R (2010) Glutamate Receptor Ion Channels: Structure, Regulation, and Function. Pharmacol Rev 62:405–496.
Tsai CH, Huang HC, Liu BL, Li CI, Lu MK, Chen X, Tsai MC, Yang YW, Lane HY (2014) Activation of N-methyl-D-aspartate receptor glycine site temporally ameliorates neuropsychiatric symptoms of Parkinson's disease with dementia. Psychiatry Clin Neurosci 68:692–700.
Vergnano AM, Rebola N, Savtchenko LP, Pinheiro PS, Casado M, Kieffer BL, Rusakov DA, Mulle C, Paoletti P (2014) Zinc dynamics and action at excitatory synapses. Neuron 82:1101–1114.
Wang H-X, Gao W-J (2010) Development of calcium-permeable AMPA receptors and their correlation with NMDA receptors in fast-spiking interneurons of rat prefrontal cortex. J Physiol 588:2823–2838.
Wang LP, Li F, Wang D, Xie K, Wang D, Shen X, Tsien JZ (2011) NMDA receptors in dopaminergic neurons are crucial for habit learning. Neuron 72:1055–1066.
Watabe-Uchida M, Zhu L, Ogawa SK, Vamanrao A, Uchida N (2012) Whole-brain mapping of direct inputs to midbrain dopamine neurons. Neuron 74:858–873.
Wild AR, Bollands M, Morris PG, Jones S (2015) Mechanisms regulating spill-over of synaptic glutamate to extrasynaptic NMDA receptors in mouse substantia nigra dopaminergic neurons. Bolam P, ed. Eur J Neurosci 42:2633–2643.
Wong JM, Folorunso OO, Barragan E V., Berciu C, Harvey TL, Coyle JT, Balu DT, Gray JA (2020) Postsynaptic Serine Racemase Regulates NMDA Receptor Function. The Journal of Neuroscience 40:9564–9575.
Yang Q, Zhu G, Liu D, Ju JG, Liao ZH, Xiao YX, Zhang Y, Chao N, Wang J, Li W, Luo JH, Li ST (2017) Extrasynaptic NMDA receptor dependent long-term potentiation of hippocampal CA1 pyramidal neurons. Sci Rep 7:1–9.
Yao L, Rong Y, Ma X, Li H, Deng D, Chen Y, Yang S, Peng T, Ye T, Liang F, Xu N, Zhou Q (2022) Extrasynaptic NMDA Receptors Bidirectionally Modulate Intrinsic Excitability of Inhibitory Neurons. Journal of Neuroscience 42:3066–3079.
Yi F, Bhattacharya S, Thompson CM, Traynelis SF, Hansen KB (2019) Functional and pharmacological properties of triheteromeric GluN1/2B/2D NMDA receptors. Journal of Physiology 597:5495–5514.
Zheng F, Lammert K, Nixdorf-Bergweiler BE, Steigerwald F, Volkmann J, Alzheimer C (2011) Axonal failure during high frequency stimulation of rat subthalamic nucleus. Journal of Physiology 589:2781–2793.

Zweifel LS, Parker JG, Lobb CJ, Rainwater A, Wall VZ, Fadok JP, Darvas M, Kim MJ, Mizumori SJ, Paladini CA, Phillips PE, Palmiter RD (2009) Disruption of NMDAR-dependent burst firing by dopamine neurons provides selective assessment of phasic dopamine-dependent behavior. Proc Natl Acad Sci U S A 106:7281–7288.

Fig 1

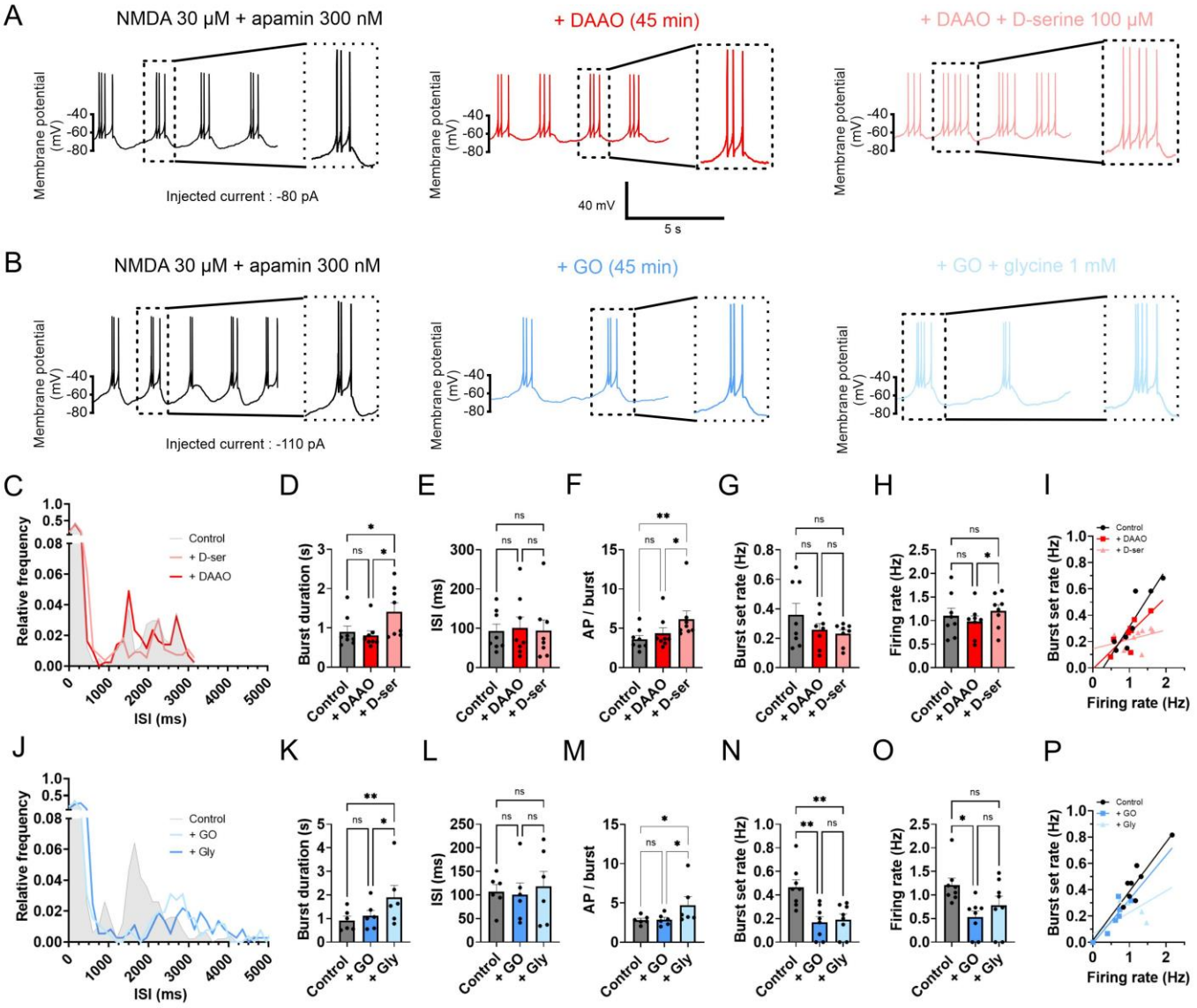
A
NMDA 30 µM + apamin 300 nM
+ DAAO (45 min)
+ DAAO + D-serine 100 µM
Membrane potential (mV)
-40
-60
-80
Injected current : -80 pA
40 mV
5 s
B
NMDA 30 µM + apamin 300 nM
+ GO (45 min)
+ GO + glycine 1 mM
Injected current : -110 pA
C
Relative frequency
Control
+ D-ser
+ DAAO
ISI (ms)
D
Burst duration (s)
E
ISI (ms)
F
AP / burst
G
Burst set rate (Hz)
H
Firing rate (Hz)
I
Burst set rate (Hz)
Firing rate (Hz)
J
Relative frequency
Control
+ GO
+ Gly
ISI (ms)
K
Burst duration (s)
L
ISI (ms)
M
AP / burst
N
Burst set rate (Hz)
O
Firing rate (Hz)
P
Burst set rate (Hz)
Firing rate (Hz)
ns
*
**

Fig 2

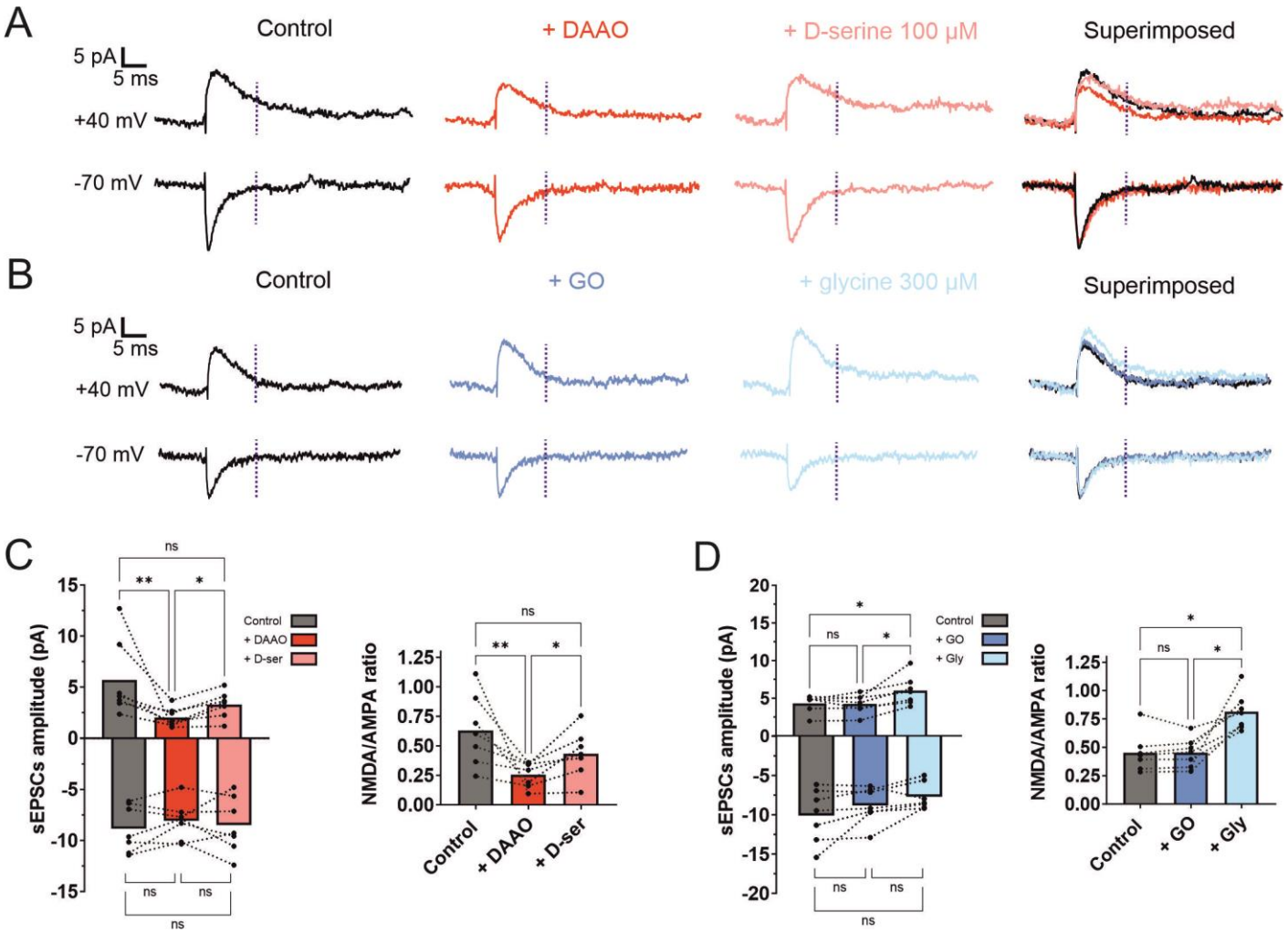
A
Control
+ DAAO
+ D-serine 100 µM
Superimposed
5 pA
5 ms
+40 mV
-70 mV
B
Control
+ GO
+ glycine 300 µM
Superimposed
5 pA
5 ms
+40 mV
-70 mV
C
sEPSCs amplitude (pA)
Control
+ DAAO
+ D-ser
ns
**
*
NMDA/AMPA ratio
Control
+ DAAO
+ D-ser
D
sEPSCs amplitude (pA)
Control
+ GO
+ Gly
NMDA/AMPA ratio
Control
+ GO
+ Gly

Fig 3

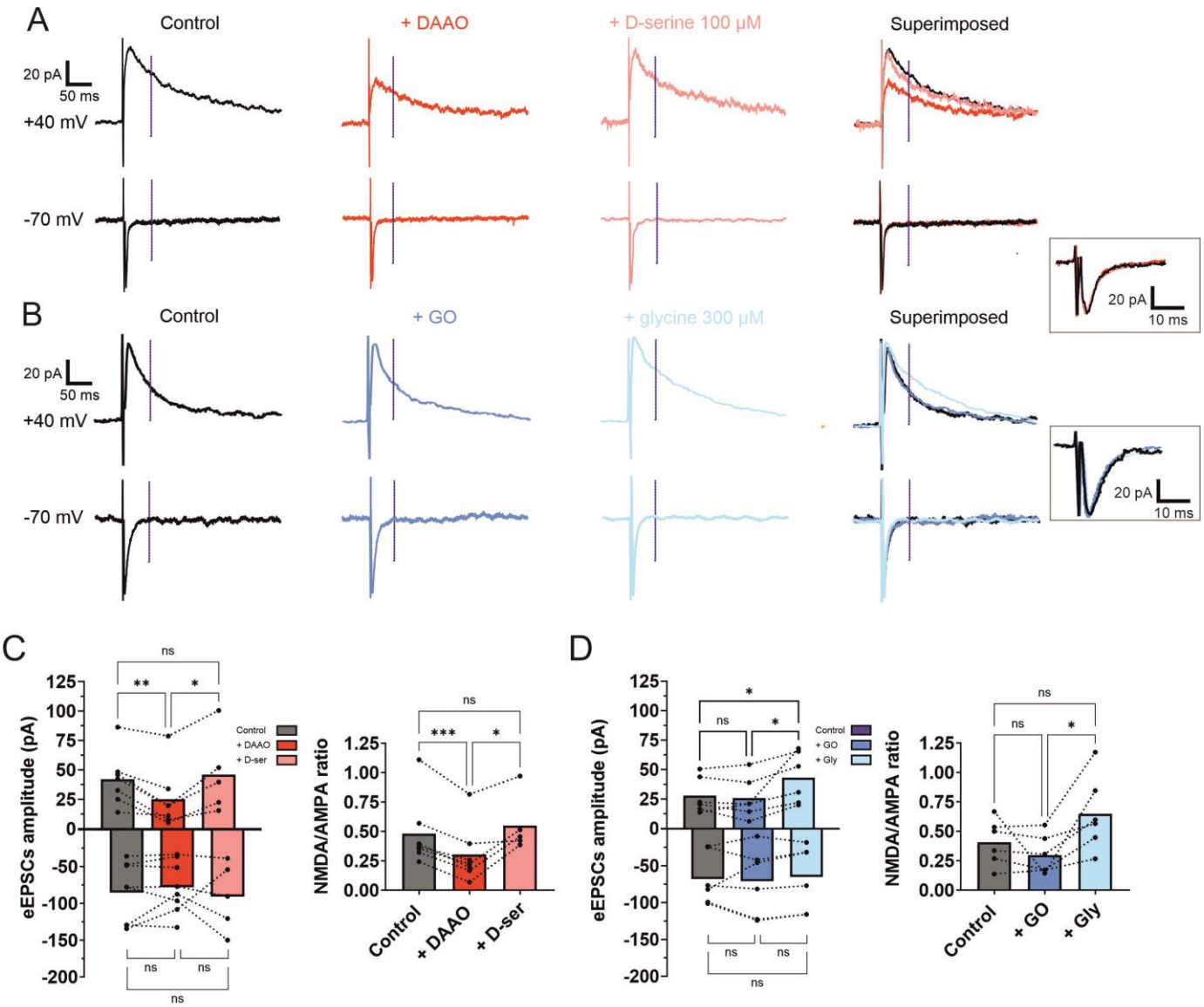
A
Control
+ DAAO
+ D-serine 100 µM
Superimposed
20 pA
50 ms
+40 mV
-70 mV
20 pA
10 ms
B
Control
+ GO
+ glycine 300 µM
Superimposed
20 pA
50 ms
+40 mV
-70 mV
20 pA
10 ms
C
eEPSCs amplitude (pA)
Control
+ DAAO
+ D-ser
NMDA/AMPA ratio
Control
+ DAAO
+ D-ser
D
eEPSCs amplitude (pA)
Control
+ GO
+ Gly
NMDA/AMPA ratio
Control
+ GO
+ Gly

Fig 4

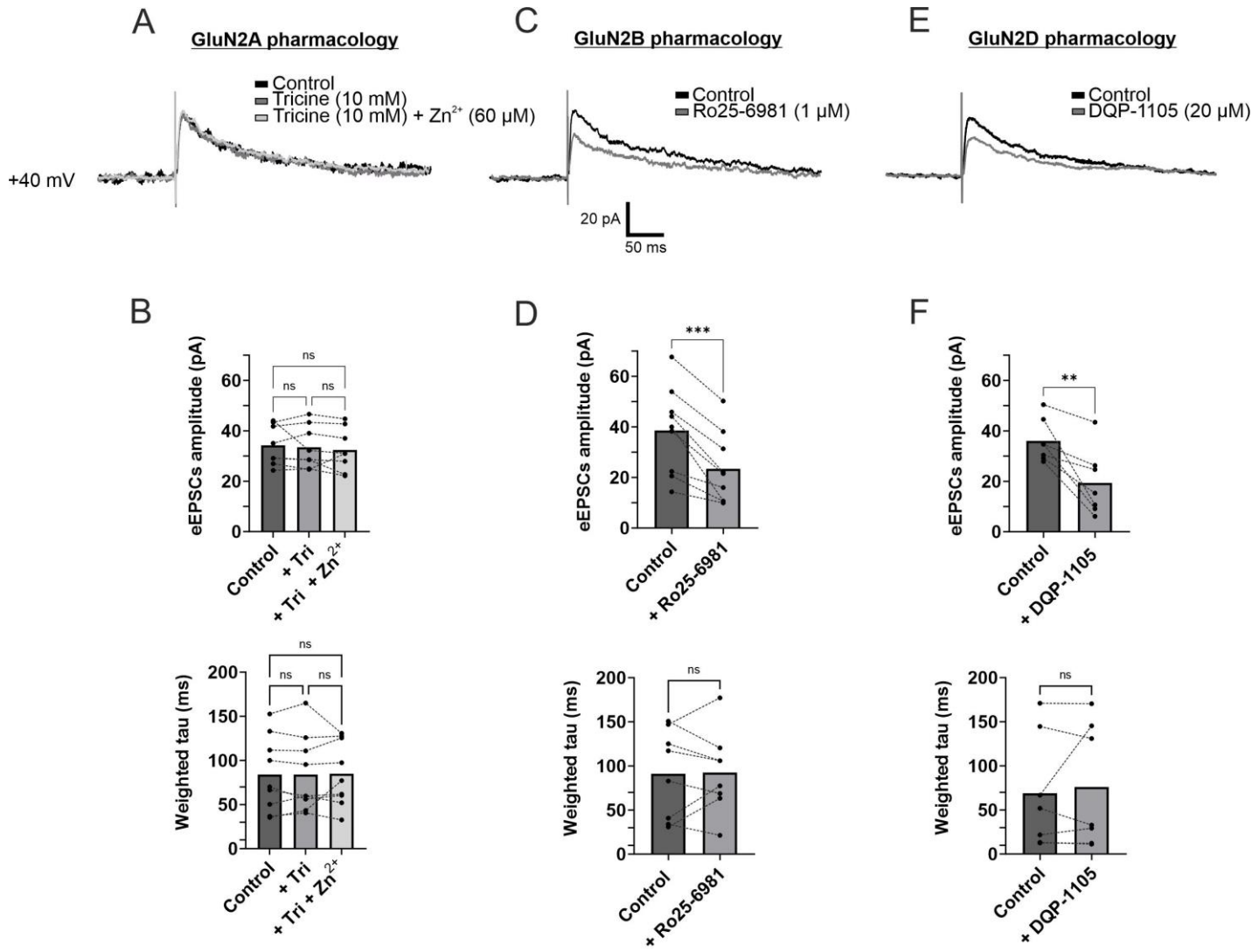
A
GluN2A pharmacology
Control
Tricine (10 mM)
Tricine (10 mM) + Zn2+ (60 μM)
+40 mV
C
GluN2B pharmacology
Control
Ro25-6981 (1 μM)
20 pA
50 ms
E
GluN2D pharmacology
Control
DQP-1105 (20 μM)
B
eEPSCs amplitude (pA)
ns
ns
ns
Control
+ Tri
+ Tri + Zn2+
Weighted tau (ms)
D
eEPSCs amplitude (pA)
***
Control
+ Ro25-6981
Weighted tau (ms)
ns
F
eEPSCs amplitude (pA)
**
Control
+ DQP-1105
Weighted tau (ms)
ns

Fig 5

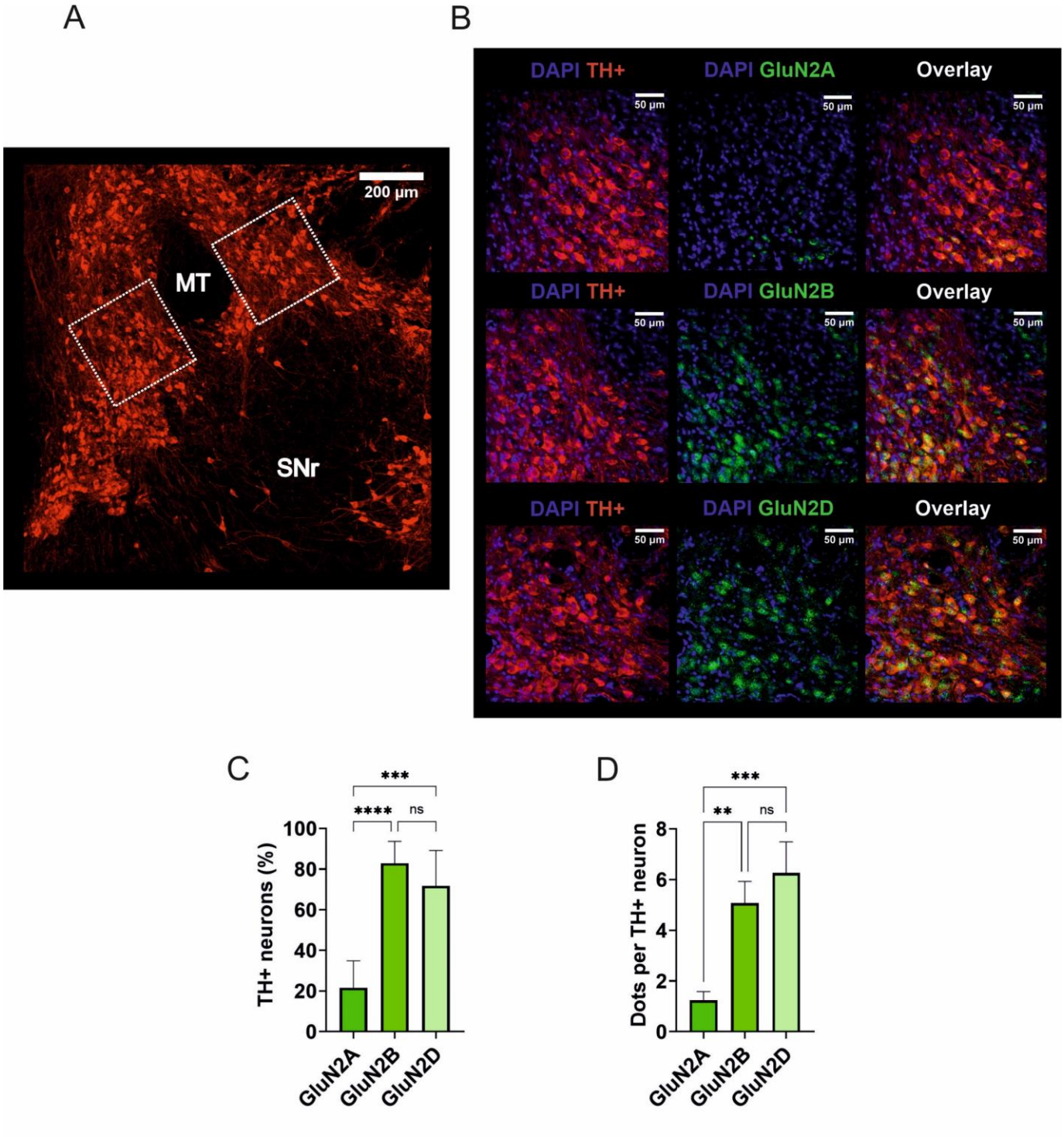
A
200 µm
MT
SNr
B
DAPI TH+
DAPI GluN2A
Overlay
DAPI TH+
DAPI GluN2B
Overlay
DAPI TH+
DAPI GluN2D
Overlay
50 µm
C
TH+ neurons (%)
100
80
60
40
20
0
***
****
ns
GluN2A
GluN2B
GluN2D
D
Dots per TH+ neuron
8
6
4
2
0
***
**
ns
GluN2A
GluN2B
GluN2D

Fig 6

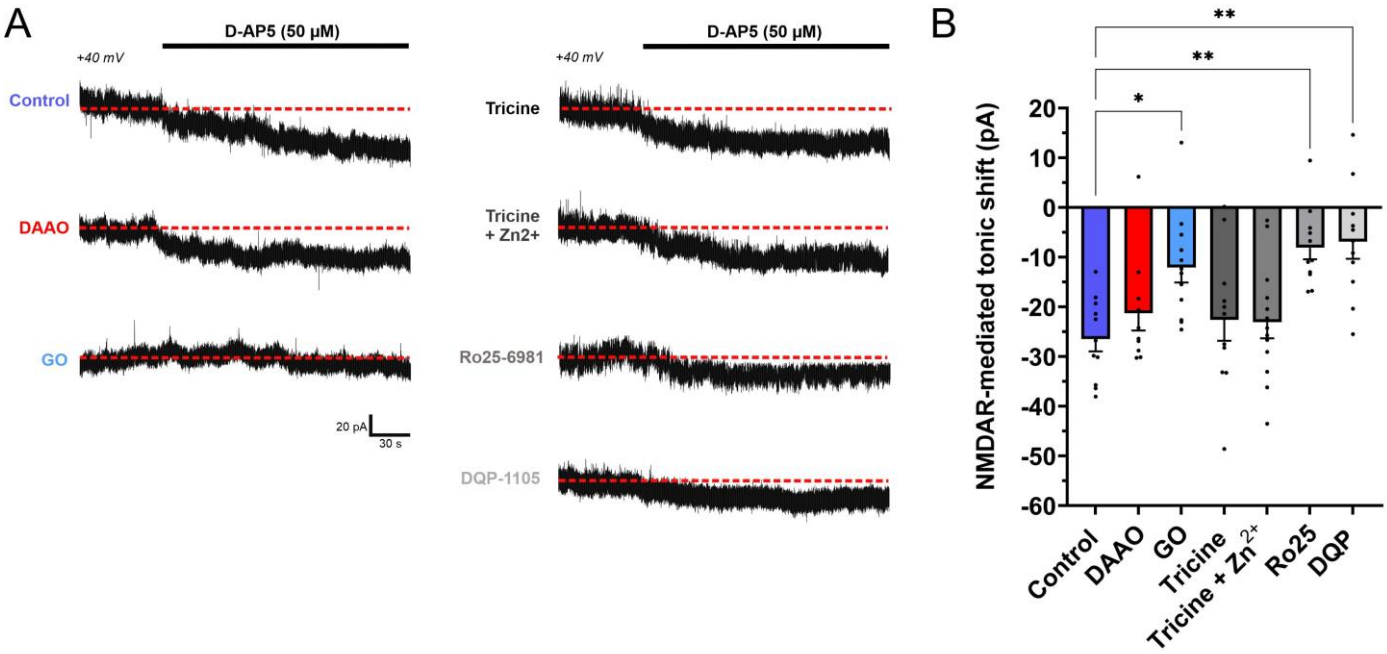
A
D-AP5 (50 μM)
+40 mV
Control
DAAO
GO
20 pA
30 s
D-AP5 (50 μM)
+40 mV
Tricine
Tricine
+ Zn2+
Ro25-6981
DQP-1105
B
NMDAR-mediated tonic shift (pA)
20
10
0
-10
-20
-30
-40
-50
-60
*
**
**
Control
DAAO
GO
Tricine
Tricine + Zn2+
Ro25
DQP

Fig 7

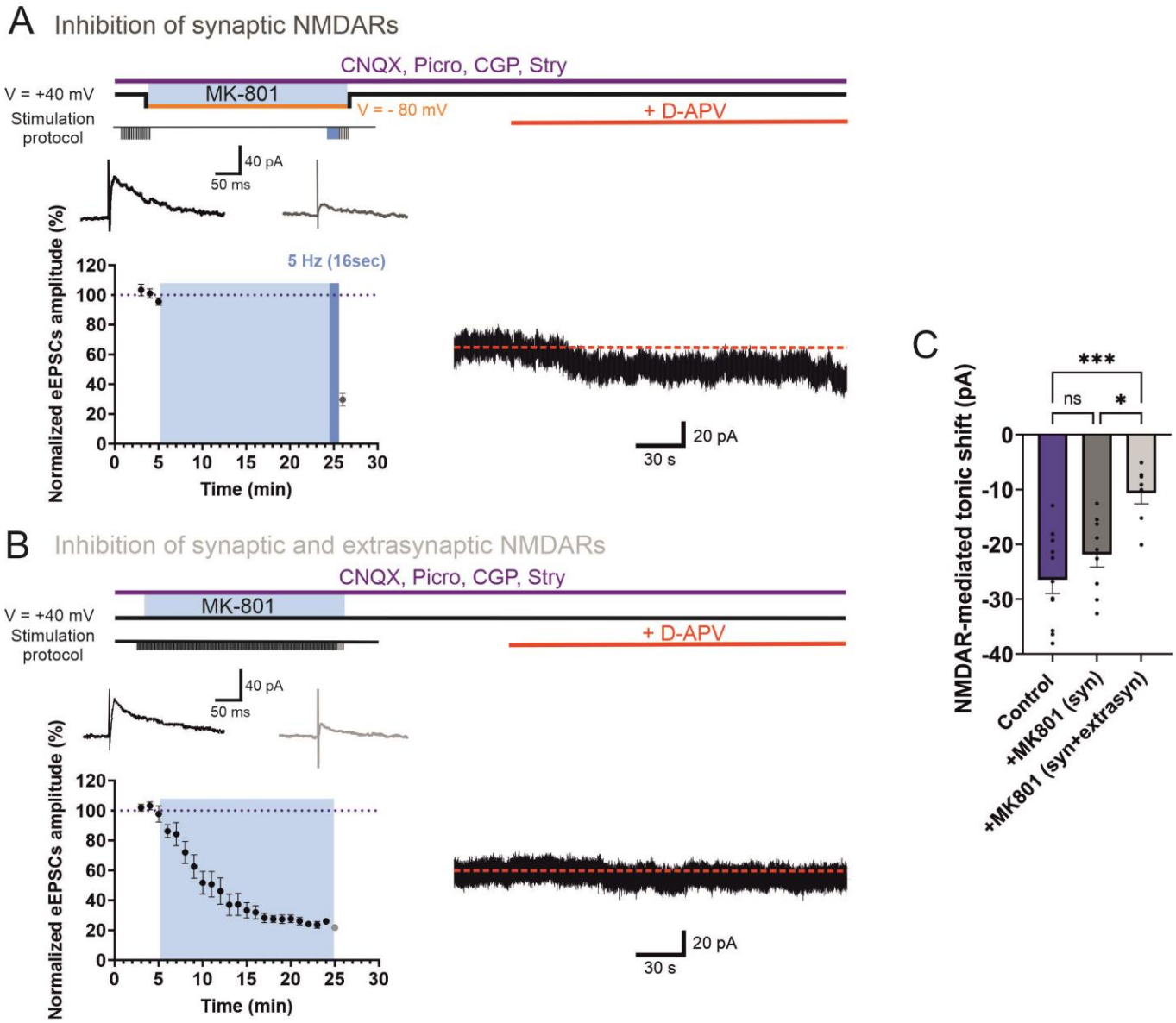
A
Inhibition of synaptic NMDARs
CNQX, Picro, CGP, Stry
V = +40 mV
MK-801
V = - 80 mV
+ D-APV
Stimulation protocol
40 pA
50 ms
5 Hz (16sec)
Normalized eEPSCs amplitude (%)
Time (min)
20 pA
30 s
B
Inhibition of synaptic and extrasynaptic NMDARs
CNQX, Picro, CGP, Stry
V = +40 mV
MK-801
+ D-APV
Stimulation protocol
40 pA
50 ms
Normalized eEPSCs amplitude (%)
Time (min)
20 pA
30 s
C
NMDAR-mediated tonic shift (pA)
***
ns
*
Control
+MK801 (syn)
+MK801 (syn+extrasyn)

Fig 8

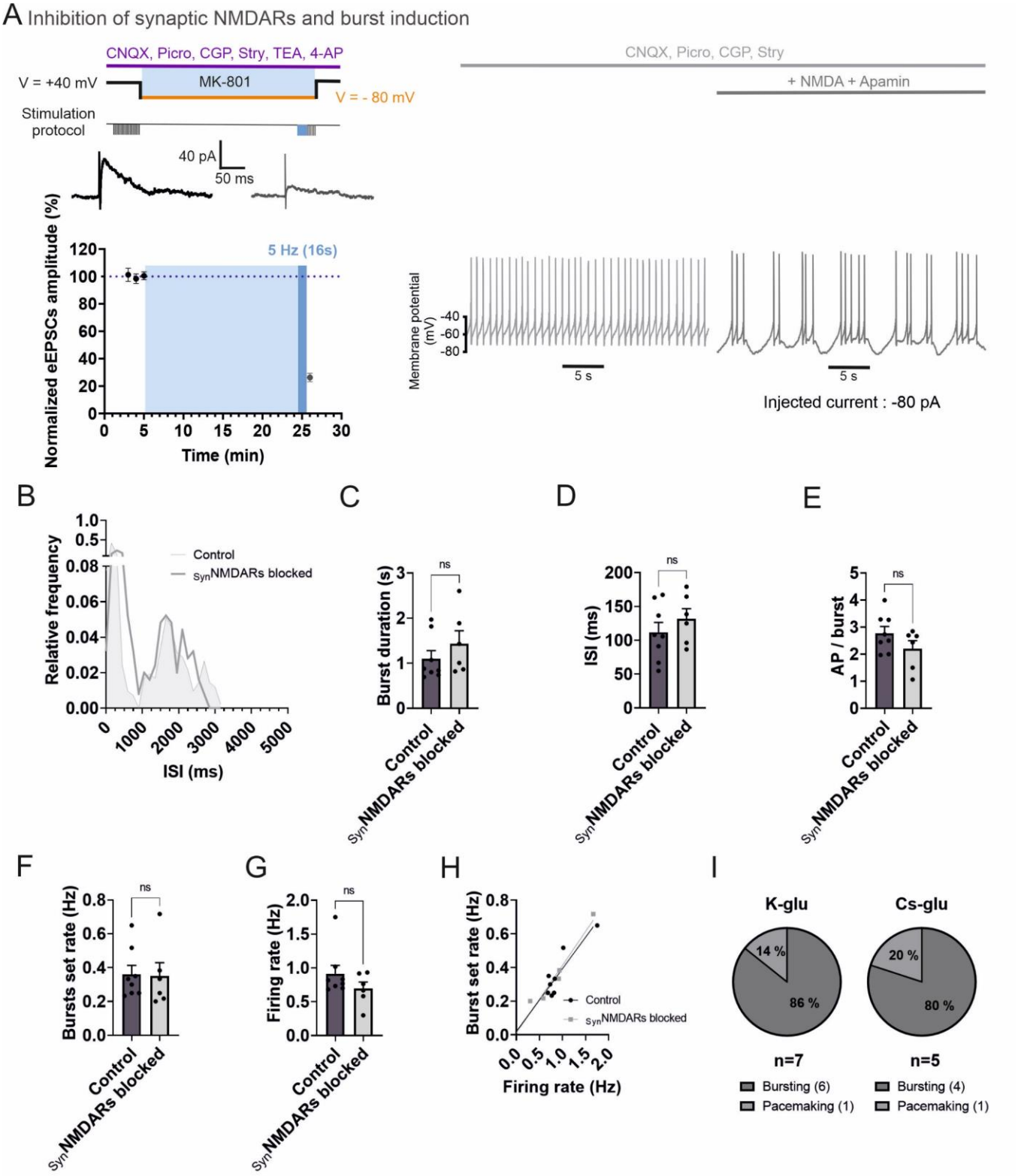
A Inhibition of synaptic NMDARs and burst induction
CNQX, Picro, CGP, Stry, TEA, 4-AP
V = +40 mV
MK-801
V = - 80 mV
Stimulation protocol
40 pA
50 ms
Normalized eEPSCs amplitude (%)
5 Hz (16s)
Time (min)
CNQX, Picro, CGP, Stry
+ NMDA + Apamin
Membrane potential (mV)
5 s
Injected current : -80 pA
B
Relative frequency
Control
SynNMDARs blocked
ISI (ms)
C
Burst duration (s)
ns
D
ISI (ms)
E
AP / burst
F
Bursts set rate (Hz)
G
Firing rate (Hz)
H
Burst set rate (Hz)
Firing rate (Hz)
I
K-glu
Cs-glu
14 %
86 %
20 %
80 %
n=7
n=5
Bursting (6)
Pacemaking (1)
Bursting (4)
Pacemaking (1)

Table 1 . Effects of enzymatic treatment with DAAO and GO on bursting activity parameters

Experimental conditions	Burst duration (s)	ISI (ms)	AP/burst	Burst set rate (Hz)	Firing rate (Hz)	slope	R2	P value of slope
Control (N=6)	0.90 ± 0.15	92.64 ± 17.92	3.61 ± 0.48	0.36 ± 0.08	1.10 ± 0.16	0.44 ± 0.09	0.81	0.0025
DAAO (n= 6)	0.81 ± 0.12 (p = 0.6171)	101.30 ± 27.42 (p = 0.9484)	4.34 ± 0.72 (p = 0.9519)	0.26 ± 0.04 (p = 0.1376)	0.98 ± 0.12 (p = 0.2435)	0.27 ± 0.09	0.62	0.0200
DAAO + D-Serine (100 µM) (n= 6)	1.41 ± 0.23 (p = 0.0124)	93.85 ± 27.52 (p = 0.9981)	6.16 ± 1.05 (p = 0.0014)	0.23 ± 0.03 (p = 0.1684)	1.21 ± 0.13 (p = 0.5762)	0.07 ± 0.08	0.12	0.4089
Control (n= 8)	0.92 ± 0.18	107.40 ± 14.93	2.84 ± 0.22	0.47 ± 0.06	1.21 ± 0.15	0.37 ± 0.08	0.79	0.0034
GO (n= 8)	1.11 ± 0.23 (p = 0.7976)	100.70 ± 24.69 (p = 0.9801)	2.87 ± 0.29 (p > 0.9999)	0.17 ± 0.05 (p = 0.0042)	0.53 ± 0.13 (p = 0.0179)	0.34 ± 0.06	0.83	0.0016
GO + glycine (1 mM) (n= 8)	1.90 ± 0.51 (p = 0.0190)	117.90 ± 31.93 (p = 0.9521)	4.71 ± 1.10 (p = 0.0281)	0.19 ± 0.05 (p = 0.0053)	0.78 ± 0.19 (p = 0.2404)	0.16 ± 0.07	0.45	0.0668

Numerical values are given as mean ± SEM P value regarding the control

Table 2 . Effects of time and blockade of synaptic NMDARs on bursting activity parameters

Experimental conditions	Burst duration (s)	ISI (ms)	AP/burst	Burst set rate (Hz)	Firing rate (Hz)	slope	R2	P value of slope
Control 0 min (N=8)	1.10 ± 0.18	111.70 ± 14.68	2.78 ± 0.25	0.36 ± 0.05	0.91 ± 0.13	0.37 ± 0.08	0.80	0.0027
Control 45 min (n= 8)	1.15 ± 0.18 (p = 0.8438)	105.20 ± 13.37 (p = 0.6917)	2.95 ± 0.33 (p = 0.3294)	0.29 ± 0.05 (p = 0.1752)	0.79 ± 0.09 (p = 0.2656)	0.36 ± 0.15	0.51	0.0477
synNMDAR blocked (n= 6)	1.43 ± 0.29 (p = 0.2824)	131.70 ± 14.98 (p = 0.3670)	2.20 ± 0.30 (p = 0.1636)	0.35 ± 0.08 (p = 0.9106)	0.69 ± 0.10 (p = 0.2824)	0.40 ± 0.05	0.95	0.0010

Numerical values are given as mean ± SEM P value regarding the control